

**$\alpha$ -ENHANCED INTEGRATED LICK/IDS SPECTRAL  
INDICES  
AND MILKY WAY AND M31 GLOBULAR CLUSTERS  
AND EARLY-TYPE GALAXIES**

Hyun-chul Lee & Guy Worthey

*Department of Physics and Astronomy, Washington State University, Pullman, WA  
99164-2814*

**ABSTRACT**

All 25 Lick/IDS spectral indices have been computed for the integrated light of simple stellar populations over broad ranges of age and metallicity and with effects from horizontal-branch stars fully implemented. Our models employ  $\alpha$ -enhanced isochrones at the sub-solar metallicity regime, but solar-scaled ones at solar and super-solar metallicity. We have also employed the updated response functions of Houdashelt et al. at the solar and super-solar metallicity regime, so that we could assess the light-element enhancement phenomena seen from metal-rich early-type galaxies. For Balmer indices a significant response was noted for  $H\gamma$  and  $H\delta$  when  $\alpha$ -elements are enhanced, but  $H\beta$  is rather  $\alpha$ -insensitive. We also find that our 5 and 12 Gyr models of  $H\gamma$  and  $H\delta$  overlap in the metal-poor regime because of changing populations of blue horizontal-branch stars. Furthermore, for populations younger than 1 Gyr, Balmer lines become weaker in the metal-poor regime because the main-sequence turnoff is hotter than 10,000 K. We present models at fixed  $[\text{Fe}/\text{H}]$  (rather than fixed heavy element mass fraction  $Z$ ) and compare to Milky Way globular clusters that have independently estimated mean  $[\text{Fe}/\text{H}]$  and  $[\alpha/\text{Fe}]$ . Comparison of our models with observations of Milky Way and M31 globular clusters in index-index space are favorable, tracing the observations at a model age of 12 Gyr *without any zero-point shifts* that are needed by some other models. The metallicity range of M31 globular clusters is similar to that of their Galactic counterparts. We also verify Beasley et al.'s recent hypothesis of the existence of young and intermediate-age star clusters in M31. Contrary to the literature values, the Milky Way globular cluster NGC 6553 appears more metal-rich than NGC 6528 from metal indices. We present  $H\delta$  and  $H\gamma$  Lick/IDS indices for the Lick/IDS sample of galaxies. We confirm the well-known enhancement of Mg and Na relative to Fe and Ca among early-type galaxies, and its increase with increasing velocity dispersion. There are distinct

differences between globular clusters and galaxies in diagrams involving  $\text{CN}_1$  and  $\text{CN}_2$ , hinting that the globular cluster environment may be a special one in terms of the amount of N incorporated into stars.

*Subject headings:* galaxies: evolution, galaxies: star clusters, stars: horizontal-branch

## 1. INTRODUCTION

Lick IDS spectral feature indices (Worthey et al. 1994) are measurements of the depths of some of the more obvious absorption blends in the spectra of stars and galaxies. They have been widely used to derive the mean age and mean chemical compositions of stellar systems such as star clusters and galaxies. Models for these indices, when compared with observations, can shed light on the ages and chemical compositions of objects as small (and local) as globular clusters to objects as large (and cosmological) as giant elliptical galaxies. As new model ingredients become available it is essential to continue to validate the use of the integrated Lick IDS spectral indices for age and metallicity estimation, especially for distant, unresolved stellar systems. One way is through the satisfactory confirmation of age and metallicity of the Milky Way globular clusters (GCs) with their independently acquired age and metallicity (e.g., Gibson et al. 1999).

In order to compute the theoretical integrated Lick IDS spectral indices for simple stellar populations (SSPs; clusterlike populations characterized by a single age and a single abundance at birth), two components are generally needed. They are (1) stellar evolutionary tracks or isochrones and (2) some connection to observable quantities such as synthetic stellar fluxes or empirically derived index fitting functions. The fitting functions of Worthey et al. (1994)<sup>1</sup> have been built upon the Lick stellar library of Milky Way stars. Because of the empirical nature of the fits, we expect that the fitting functions follow the abundance pattern of the stars to which they were fit. That is, in the metal-poor regime ( $[\text{Fe}/\text{H}] < 0.0$ ) they should represent stars of  $[\alpha/\text{Fe}] \sim +0.3$  dex and at the solar and super-solar metallicity regime they represent stars of  $[\alpha/\text{Fe}] \approx 0.0$ .

Bearing this in mind, we employ  $\alpha$ -enhanced isochrones at subsolar metallicities (in this work  $Y^2$  isochrones, Kim et al. 2002) in order to make SSP models that are more compatible with the  $\alpha$ -element enhanced fitting functions. By the same token, we compute our models using solar-scaled  $Y^2$  isochrones in the solar and super-solar metallicity regime. Also, in

---

<sup>1</sup>See also Worthey & Ottaviani (1997) for  $\text{H}\delta_A$ ,  $\text{H}\gamma_A$ ,  $\text{H}\delta_F$ ,  $\text{H}\gamma_F$ .

order to make a straightforward comparison with observational data, we present our model results as a function of  $[\text{Fe}/\text{H}]$  instead of as a function of total metallicity,  $[\text{Z}/\text{H}]$  (cf. Trager et al. 2000a; Thomas, Maraston, & Bender 2003a; hereafter TMB03a).

Besides basic checking of our models with wide variety of data, some of the issues that we are addressing in this study are the following: (1) the sensitivity of the bluer Balmer indices,  $\text{H}\gamma$  and  $\text{H}\delta$ , to  $\alpha$ -enhancement may be higher than for  $\text{H}\beta$  (Thomas, Maraston, & Korn 2004), (2) young and intermediate-age star clusters may be present in M31 (Beasley et al. 2004, 2005; Burstein et al. 2004), (3) there may be CN anomaly between GCs and early-type galaxies (Burstein et al. 1984), (4) the overall Mg enhancement in early-type galaxies is seen to depend on velocity dispersion (Worthey 1998, Worthey, Faber, & González 1992), and (5) there may be a Ca underabundance in early-type galaxies compared to the solar mixture (Thomas, Maraston, & Bender 2003b; Cenarro et al. 2004).

In the following section, we describe our models in detail. In § 3 we compare models with recent observations of Milky Way and M31 globular clusters and early-type galaxies. Section 4 summarizes and concludes our work.

## 2. STELLAR POPULATION MODELS

The present models are direct descendents of an evolutionary population synthesis code that was developed to study the stellar populations of globular clusters and early-type galaxies (Lee, Yoon, & Lee 2000; Lee, Lee, & Gibson 2002). In this work, we have taken advantage of a recent emergence of the  $Y^2$  isochrones with an  $\alpha$ -mixture [this mixture has O, Ne, Na, Mg, Si, P, S, Cl, Ar, Ca, and Ti enhanced and Al and Mn depressed relative to Fe, C, N, K, Cr, and Ni: cf. Kim et al. (2002)]. This mixture may not track the halo abundance exactly, but it should be fairly closely compatible with the stellar library that was the basis of Worthey et al. (1994)’s fitting functions, at least at the metal-poor end. We assume that the the behavior of the library is roughly:  $[\alpha/\text{Fe}] = +0.3$  for  $[\text{Fe}/\text{H}] < -1.0$ ,  $[\alpha/\text{Fe}]$  goes from  $+0.3$  to  $0.0$  as  $[\text{Fe}/\text{H}]$  does from  $-1.0$  to  $0.0$ , and  $[\alpha/\text{Fe}] = 0.0$  for  $[\text{Fe}/\text{H}] > 0.0$  (e.g., Wheeler, Sneden, & Truran 1989).

Following earlier work (Lee et al. 2000, 2002), we take into account the detailed systematic variation of horizontal-branch (HB) morphology with age and metallicity. The post-red giant branch evolutionary tracks by Yi, Demarque, & Kim (1997) are coupled to the  $Y^2$  isochrones. In order to reproduce the observational HB morphology of Milky Way globular clusters, a value of  $\eta = 0.6$  was taken, where  $\eta$  is the scaling factor in the Reimers (1975) formula for stellar mass loss. The value of the helium enrichment parameter,  $\Delta Y/\Delta Z = 2$ ,

was assumed. The standard Salpeter (1955) initial mass function was adopted for calculating the relative number of stars along the isochrones. The investigated age range is from 1 Gyr to 12 Gyr and the metallicities cover  $-2.5 \leq [\text{Fe}/\text{H}] \leq +0.5$ .

The strength of spectral line indices is calculated with either

$$EW = \Delta\lambda(1 - (F_\lambda/F_C)) \quad (1)$$

or

$$Mag = -2.5\log(F_\lambda/F_C), \quad (2)$$

where  $\Delta\lambda$  is an index bandpass and  $F_\lambda$  and  $F_C$  are the flux in the index bandpass and the pseudocontinuum flux in the index bandpass (Worthey et al. 1994; Worthey & Ottaviani 1997). First, for each star (or bin of stars along an isochrone) with a given metallicity, temperature, and gravity, we find the average flux values within both pseudocontinuum regions for each index from the stellar model atmospheres. We have employed the stellar model atmospheres of Lejeune, Cuisinier, & Buser (1997, 1998) in this study to place  $F_C$ . We derive  $F_C$  at the center of each index bandpasses by linear interpolation in wavelength. Second, we calculate either the equivalent width (EW; e.g., for  $\text{H}\beta$ ) or the magnitude (Mag; e.g., for  $\text{Mg}_2$ ) using Worthey et al. (1994) and Worthey & Ottaviani (1997) fitting functions, where the index value is given as a function of stellar  $[\text{Fe}/\text{H}]$ , temperature, and gravity. This allows one to solve for  $F_\lambda$ . Finally, we sum  $F_C$  and  $F_\lambda$  over all bins in the isochrone and compute the integrated strengths of spectral feature indices using equations (1) and (2).

We want to stress that our models are presented at fixed  $[\text{Fe}/\text{H}]$  so that it can be compared directly to observed integrated cluster spectral feature indices in the cases where the cluster has independently-measured mean  $[\text{Fe}/\text{H}]$  and  $[\alpha/\text{Fe}]$ . Thomas & Maraston (2003) and Maraston et al. (2003) have recently investigated the impact of  $\alpha$ -enhanced stellar evolutionary tracks on stellar population models using the evolution of Salasnich et al. (2000). One should realize, however, that because their models are provided at fixed total metallicity  $[\text{Z}/\text{H}]$ , they find that  $\alpha$ -enhanced tracks are hotter than solar-scaled ones, mostly owing to the lower opacities of  $\alpha$ -enhanced stellar atmospheres at fixed total metallicity  $[\text{Z}/\text{H}]$ . The situation is opposite for models given at fixed  $[\text{Fe}/\text{H}]$ : the  $\alpha$ -enhanced tracks are cooler at a given  $[\text{Fe}/\text{H}]$  (cf. Figures 2 and 3 of Kim et al. 2002).

In order to investigate  $\alpha$ -enhancement at solar and super-solar metallicities where many massive elliptical galaxies reside, we employ scaled-solar isochrones, but include modifications to the Lick IDS index strengths based on the updated response functions (RFs) by Houdashelt et al. (2002) which we describe in detail in the following.

Recently, Houdashelt et al. (2002; hereafter HTWB02) repeated and expanded the earlier work of Tripicco & Bell (1995; hereafter TB95) on the sensitivity of each Lick spectral

index as the abundances of individual chemical elements are varied. They used revised and updated spectral line lists, including TiO bands that were not included in TB95. In addition, they added the age-sensitive H $\gamma$  and H $\delta$  indices<sup>2</sup>.

HTWB02’s experiments, like those of TB95, are done only at solar metallicity and only for three evolutionary phases. We apply this treatment at the solar and super-solar regime (in our tabulated models, the [Fe/H] = 0.0 and +0.5 entries are modified). Hence, even though our default models at [Fe/H] = 0.0 and +0.5 have isochrones with [ $\alpha$ /Fe] = 0.0, with the help from HTWB02 we can appraise  $\alpha$ -element enhancement phenomena in the limit where the abundance mixture does not feed back to change isochrone shape or number distribution. We do not, however, apply this treatment at the sub-solar regime because we assume that the regular fitting functions follow the Milky Way abundance pattern.

For metal-rich indices, we include enhancement effects from the chemical elements O, Na, Mg, Si, Ca, and Ti, while elements C, N, and Cr track Fe in a scaled-solar fashion. This (1) accommodates the general observational trends seen from globular cluster stars (e.g., Fig. 14 of Ramírez & Cohen 2003) and (2) mimics the  $\alpha$ -mixture of the  $Y^2$  isochrones (Fig. 1 of Kim et al. 2002). Detailed studies for the C- and N-sensitive indices are under way and will be presented elsewhere. Therefore, and despite the fact that we know this does not fit all observations, the model indices CN<sub>1</sub>, CN<sub>2</sub>, G4300, C<sub>2</sub>4668 that we present in this paper assume approximately scaled-solar behavior for C and N.

### 3. COMPARISON WITH OBSERVATIONS

#### 3.1. COMPARISON WITH MILKY WAY GLOBULAR CLUSTERS

Having discussed the theoretical aspects of generating the integrated  $\alpha$ -enhanced Lick spectral indices in § 2, we now provide empirical checks of our models using Milky Way GCs. In this work, we use two datasets for the Milky Way GCs. One is from Cohen, Blakeslee,

---

<sup>2</sup>The tables of spectral index response to abundance changes are available at the <http://astro.wsu.edu/hclee/HTWB02>. Also, please refer to section 3.3 in Worthey (2004) to find the differences between TB95 and HTWB02.

& Ryzhov (1998)<sup>3</sup> and the other is from Puzia et al. (2002)<sup>4</sup>. We use the Harris (1996) compilation<sup>5</sup> for [Fe/H] of the Milky Way GCs. Figures 1–6 show [Fe/H] vs. Lick indices in order to take advantage of independent measurements of mean [Fe/H] and  $[\alpha/\text{Fe}]$  of the Milky Way GCs.

For models in Figures 1 and 2,  $[\alpha/\text{Fe}] = +0.3$  dex  $Y^2$  isochrones are employed at [Fe/H] =  $-2.5$ ,  $-2.0$ ,  $-1.5$ , and  $-1.0$ , while  $[\alpha/\text{Fe}] = +0.15$  dex  $Y^2$  isochrones are used at [Fe/H] =  $-0.5$ , and, finally, solar-scaled  $Y^2$  isochrones with HTWB02 response functions of [O,Na,Mg,Si,Ca,Ti/Fe] =  $+0.3$  dex are applied at [Fe/H] =  $0.0$  and  $+0.5$ . The effects from blue HB stars are clear as 10 Gyr and 12 Gyr lines are compared at the metal-poor regime. It is also noted that Balmer lines become weaker with decreasing metallicity at 1 Gyr because the main-sequence turnoff becomes hotter than 10,000 K in metal-poor populations.

In Figures 1-6, the data of Cohen et al. (C98, circles) are, from the left<sup>6</sup>, and with [Fe/H] values (Harris 1996) noted in parentheses, NGC 6341 (M92;  $-2.28$ ), NGC 6205 (M13;  $-1.54$ ), NGC 6121 (M4;  $-1.20$ ), NGC 6838 ( $-0.73$ ), NGC 6539 ( $-0.66$ ), NGC 6760 ( $-0.52$ ), NGC 6356 ( $-0.50$ ), NGC 6624 ( $-0.44$ ), NGC 6440 ( $-0.34$ ), NGC 6553 ( $-0.21$ ), and NGC 6528 ( $-0.04$ ). Those of Puzia et al. (P02, triangles) are, from the left, NGC 6218 (M12;  $-1.48$ ), NGC 6626 (M28;  $-1.45$ ), NGC 6981 (M72;  $-1.40$ ), NGC 6284 ( $-1.32$ ), NGC 6637 ( $-0.70$ ), NGC 6388 ( $-0.60$ ), NGC 6441 ( $-0.53$ ), NGC 6356 ( $-0.50$ ), NGC 6624 ( $-0.44$ ), NGC 5927 ( $-0.37$ ), NGC 6553 ( $-0.21$ ), and NGC 6528 ( $-0.04$ ). There are 4 GCs in common between C98 and P02. They are NGC 6356 ([Fe/H] =  $-0.50$ ), NGC 6624 ([Fe/H] =  $-0.44$ ), NGC 6553 ([Fe/H] =  $-0.21$ ), and NGC 6528 ([Fe/H] =  $-0.04$ ). It is useful to note that the latter two are among the most metal-rich Galactic globular clusters because it would be interesting to find if even more metal-rich GCs than these exist in other galaxies.

From Figures 1 and 2, where we compare C98 and P02 datasets of Milky Way GCs with our Balmer line models, we find a good overall agreement and clear emergence of horizontal-

---

<sup>3</sup>In this work, we use Table 2 in Beasley et al. (2004) who remeasured the original Cohen et al. spectra with careful consideration of flux and wavelength calibration. Beasley et al. even managed to measure some of previously unmeasured Lick indices which reside at the shorter wavelength range, such as  $H\gamma_A$ ,  $H\gamma_F$ , Ca4227, G4300, Fe4383, Fe4531 as well as their errors. Due to its large uncertainty we do not use NGC 6171 (M107, [Fe/H] =  $-1.04$ ) index data. We use original C98 data for  $\text{TiO}_2$  since Beasley et al. did not measure this index.

<sup>4</sup>It is Puzia et al.'s Table D that is used in this study. For  $H\gamma$  and  $H\delta$ , their Table C is used.

<sup>5</sup><http://physun.mcmaster.ca/~harris/mwgc.dat>

<sup>6</sup>In Figure 2, in the upper panel for  $H\gamma$ , C98 data are, from the left, NGC 6341, NGC 6205, NGC 6121, NGC 6838, and NGC 6356.

branch morphology effects. We see that (1) our models of Balmer lines satisfactorily trace the observational data of Milky Way GCs at 12 Gyr without zero-point shifts throughout the metallicity range, (2) C98’s most metal-poor cluster, M92 ( $[\text{Fe}/\text{H}] = -2.28$ ) is well matched with our models, (3) C98’s M13 ( $[\text{Fe}/\text{H}] = -1.54$ , HB Type<sup>7</sup> = 0.97) and P02’s M12<sup>8</sup> ( $[\text{Fe}/\text{H}] = -1.48$ , HB Type = 0.92) with comparable metallicity and similar HB morphology are rather satisfactorily reproduced from our model Balmer line indices, (4) C98’s M4 ( $[\text{Fe}/\text{H}] = -1.20$ , HB Type =  $-0.07$ ) consistently shows strong  $\text{H}\beta$ ,  $\text{H}\gamma_A$ , and  $\text{H}\gamma_F$  as expected from its HB morphology (Lee et al. 2000).

In Figures 3–6, 12 Gyr models for non-Balmer indices are shown. At  $[\text{Fe}/\text{H}] = 0.0$  and  $+0.5$ , HTWB02 response functions of  $[\alpha/\text{Fe}] = 0.0$  (*solid lines*; our default model without HTWB02 treatment),  $+0.3$  (*dotted lines*),  $+0.6$  dex (*dashed lines*) are, respectively, employed on top of the solar-scaled  $Y^2$  isochrones.

For each metal index we first concentrate on the sub-solar metallicity regime to check our use of  $\alpha$ -enhanced  $Y^2$  isochrones for the comparably  $\alpha$ -enhanced Milky Way GCs (e.g., Carney 1996). Secondly, we inspect the sensitivity of integrated Lick metal line indices on  $\alpha$ -enhancement as we employ HTWB02 response functions at the solar and super-solar metallicity regime. To clarify our thinking we have divided the Lick metal line indices into four groups. They are (1) CN-sensitive indices  $\text{CN}_1$ ,  $\text{CN}_2$ , G4300, and  $\text{C}_24668$ , calcium-sensitive index  $\text{Ca}4227$ , and  $\text{Ca}4455$ , (2) iron-sensitive indices  $\text{Fe}4383$ ,  $\text{Fe}5270$ ,  $\text{Fe}5335$ ,  $\text{Fe}5406$ , and  $\text{Fe}5709$ , (3) Mg-sensitive indices  $\text{Mg}_1$ ,  $\text{Mg}_2$ , and  $\text{Mg } b$ , and (4) mixed-sensitivity  $\text{Fe}4531$ ,  $\text{Fe}5015$ , and  $\text{Fe}5782$ , Na-sensitive Na D, and  $\text{TiO}_1$  and  $\text{TiO}_2$ .

$\text{CN}_1$ ,  $\text{CN}_2$ : In the top left panel of Figure 3, Milky Way GCs are systematically  $\sim 0.03$  mag stronger than our models in  $\text{CN}_1$ . In  $\text{CN}_2$ , the data tilt against our models, being weaker at the metal-poor end but stronger at the metal-rich end compared to our models (similar to  $\text{TiO}_2$  in Figure 6). The  $\text{CN}_1$  and  $\text{CN}_2$  mismatch may originate from intrinsic differences between globular cluster stars and galactic field halo stars on that our models are based (e.g., Langer, Suntzeff, & Kraft 1992). The Milky Way GC stars, down to main sequence turn-off, are known to be generally different from the field halo stars in the sense that the former show some phenomena such as CH-CN bimodality (e.g., Cannon et al. 1998; Harbeck, Smith, & Grebel 2003). As TMB03a suggested, nitrogen enhancement rather than that of carbon might be helpful to alleviate the discrepancy between models and the data.

---

<sup>7</sup>HB Type is defined as  $[(\text{B} - \text{R}) / (\text{B} + \text{V} + \text{R})]$ , where B and R are the number of HB stars left and right of the instability strip, respectively, while V is the number of RR Lyrae stars (Lee, Demarque, & Zinn 1994).

<sup>8</sup>The most metal-poor GC in the P02 sample.

Also, it is noted in Tables 2 and 3 of Worthey et al. (1994) that the fitting functions for  $CN_1$  and  $CN_2$  are not valid below  $[Fe/H] = -1$  due to lack of stars in the sample over which one could model a fit. We are left, then, with too many possible explanations for CN index drift.

According to TB95 and HTWB02, both  $CN_1$  and  $CN_2$  are heavily sensitive to C and N. In this study, however, as we employ the HTWB02 treatment at the solar and super-solar metallicity regime we do not include C- and N-enhancement (see § 2). Hence, as depicted in Figure 3 both  $CN_1$  and  $CN_2$  (also G4300 and  $C_24668$ ) decrease with increasing  $\alpha$ -enhancement mostly due to O and Mg.

*G4300*: The middle left panel of Figure 3 shows that our models of G4300 competently trace C98 data, but not for some of metal-rich P02 GCs. Opposite to TMB03a models, and conceivably because we do not include C-enhancement, G4300 decreases a bit with increasing  $\alpha$ -enhancement, mostly due to O. G4300 is a C- and O-sensitive index according to TB95 and HTWB02.

*C<sub>2</sub>4668*: The middle right panel of Figure 3 depicts that our models illustriously track C98 points, while P02 GCs show a poor match as already seen in Fig. 2 of TMB03a. This is primarily a C-sensitive index, but responds negatively to O-enhancement. Contrary to TMB03a, possibly because we do not take into account C-enhancement,  $C_24668$  decreases with increasing  $\alpha$ -enhancement mostly due to increased O.

*Ca4227*: The bottom left panel of Figure 3 shows that both C98 and P02 are slightly weaker than our models at the metal-rich ( $[Fe/H] > -0.5$ ) regime. Ca4227 is a highly  $\alpha(Ca)$ -sensitive index. In fact, it is the only Ca-sensitive Lick index according to TB95 and HTWB02. Without considering the effects from C- and N-enhancement, Ca4227 significantly increases with increasing  $\alpha$ -enhancement mostly due to Ca as manifested in Figure 3 at the super-solar metallicity regime contrary to TMB03a.

*Ca4455*: Some notable mismatch is seen between Milky Way GCs and our models for Ca4455 in the bottom right panel of Figure 3. NGC 6356 ( $[Fe/H] = -0.50$ ) is the only common GC between C98 and P02 ( $C98 = 0.69 \text{ \AA}$ ,  $P02 = 1.48 \text{ \AA}$ ). We suspect that P02’s measurements are maybe erroneous because it is seen in Figure 10 that C98 extensively overlap with M31 GCs. One possibility is that Ca4455 generally requires large systematic corrections to get from modern CCD spectra back to the original Lick/IDS system (Worthey 2004). Ca4455 is misnamed in the sense that it is not an  $\alpha$ - or Ca-sensitive index at all (TB95; HTWB02). It is actually an  $\alpha$ -insensitive index as demonstrated in Figure 3.

*Fe4383*: From the upper left panel of Figure 4, it is seen that Milky Way GCs are rather well traced by our models of Fe4383 though some appear mildly weaker (by  $\sim 0.5 \text{ \AA}$ ) at around

$[\text{Fe}/\text{H}] = -0.5$  compared to our models. Nevertheless, this index is a promising substitute for the popularly used Fe5270 and Fe5335 if shorter wavelengths are available. Fe4383 an  $\alpha$ -anti-sensitive index. It decreases with increasing  $\alpha$ -enhancement, just as predicted by HTWB02. According to TB95, it is the most Fe-sensitive index (but according to HTWB02, that honor is bestowed upon Fe5335).

*Fe5270, Fe5335,  $\langle \text{Fe} \rangle$ <sup>9</sup>, Fe5406, Fe5709*: The rest of Figure 4 depicts that both C98 and P02 are fairly well tracked by our models of these Fe-sensitive line indices. It is particularly interesting to note that C98’s NGC 6553 and NGC 6528 (the last two most metal-rich GCs) seem to suggest that NGC 6553, because it has slightly stronger indices, may be slightly more metal-rich than NGC 6528, contrary to usual literature values<sup>10</sup>. Mainly because we are considering  $\alpha$ -enhancement at fixed  $[\text{Fe}/\text{H}]$ , it is noted that these Fe-sensitive indices are rather  $\alpha$ -insensitive (i.e. contrary to the appearance of plots in TMB03a).

*Mg<sub>1</sub>, Mg<sub>2</sub>, Mg b*: It is seen from Figure 5 that our models satisfactorily match both C98 and P02. Between NGC 6553 and NGC 6258, NGC 6553 is again consistently stronger than NGC 6528 in these Mg indices, according to C98. Every Mg index is highly sensitive to Mg abundance only, rather than  $\alpha$  abundance in general. They increase with increasing  $\alpha$  mostly due to Mg. Mg *b* is the most Mg-sensitive index among them.

*[MgFe]*<sup>11</sup>: The bottom right panel of Figure 5 depicts that our model of this Mg *b*, Fe5270, Fe5335 combined index successfully traces the Milky Way GCs throughout the entire metallicity range.

*Fe4531, Fe5015*: The upper right panel of Figure 6 shows that C98 are systematically weaker (by  $\sim 0.5 \text{ \AA}$ ) than our models of Fe5015 over the entire metallicity range (opposite of CN<sub>1</sub>, but similar to Ca4455 and TiO<sub>1</sub>). These two are Ti-sensitive indices according to TB95 and HTWB02. Both slightly increase with increasing  $\alpha$ -enhancement, mostly due to Ti.

*Fe5782*: In the middle left panel of Figure 6 the C98 points are relatively stronger, with large errors, compared to our models at the metal-rich regime. It is not an Fe-sensitive index but it responds negatively, albeit weakly, to increased  $\alpha$ .

*Na D*: The middle right panel of Figure 6 manifests that similar to TMB03a, our models

<sup>9</sup> $\langle \text{Fe} \rangle = (\text{Fe5270} + \text{Fe5335})/2$ .

<sup>10</sup>Barbuy et al. (2004) present  $[\text{Fe}/\text{H}] = -0.15$  for NGC6528 and  $[\text{Fe}/\text{H}] = -0.20$  for NGC6553, for instance.

<sup>11</sup> $[\text{MgFe}] = \sqrt{\text{Mg}b \times \langle \text{Fe} \rangle}$ .

are generally weaker than Milky Way GCs. Particularly, data are stronger than our models at  $-1.5 < [\text{Fe}/\text{H}] < 0.0$ . Note that the Worthey et al. (1994) fitting functions were corrected for interstellar Na D absorption, but that of the globular cluster indices have not. TMB03a suggests that the too-strong Na D indices may be due to the Na absorption in interstellar material, and this is certainly true at the level of a few tenths of an Å in equivalent width. In addition, similar to  $\text{CN}_1$  and  $\text{CN}_2$ , it is possible that Na–O anti-correlation phenomenon seen in globular cluster stars may have something to do with this mismatch (e.g., Gratton et al. 2001). Contrary to TMB03a, Na D heftily increases with increasing  $\alpha$ -enhancement mostly due to our assumed Na-enhancement, similar to Ca4227.

*TiO<sub>1</sub>, TiO<sub>2</sub>*: The bottom left panel of Figure 6 shows that C98 are systematically  $\sim 0.01$ – $0.02$  mag weaker than our models in  $\text{TiO}_1$ . For  $\text{TiO}_2$ , we use the C98 original measurements because Beasley et al. (2004) did not measure this index. Possibly because of the differences between TB95 (no molecular TiO band effects) and HTWB02, both  $\text{TiO}_1$  and  $\text{TiO}_2$  increase with increasing  $\alpha$ -enhancement due to Ti- and O-enhancement.

From the above comparisons, we conclude that  $\text{CN}_2$ , Ca4455, Fe5015, Fe5782,  $\text{TiO}_2$  may be rather ambiguous as chemical abundance indicators. It is also noted that some of metal line indices such as C<sub>2</sub>4668, Fe5335, Fe5406, Na D,  $\text{TiO}_1$ ,  $\text{TiO}_2$  do not go monotonically with  $[\text{Fe}/\text{H}]$  at the metal-poor end (i.e., they become stronger at  $[\text{Fe}/\text{H}] < -1.5$ ). It is suggested from Fig. 7 of Gibson et al. (2003) that it is of great importance to check whether the metallicities of Milky Way globular clusters are safely reproduced from the models or not before the diagnostic diagrams such as Mg *b* vs. Balmer lines are used for age estimation. With some notable exceptions, our models match the integrated feature strengths of GCs with considerable accuracy.

### 3.2. COMPARISON WITH M31 GLOBULAR CLUSTERS

Having compared and examined our  $\alpha$ -enhanced models with Milky Way GCs, we apply our models to M31 GCs. In this study, we mainly use Beasley et al. (2004) Keck observations of M31 GCs listed in their Tables 1 and 4. Among their sample of M31 GCs, they have analyzed that 6 of them are possibly young star clusters (YSCs: depicted as triangles in our plots)<sup>12</sup>, 6 of them are intermediate-age GCs (IAGCs: diamonds in our plots)<sup>13</sup>, and 6 are

---

<sup>12</sup>They are 222-277, 314-037, 321-046, 322-049, 327-053, and 380-313.

<sup>13</sup>They are 126-184, 292-010, 301-022, 337-068, NB 16, and NB 67. Please refer to Beasley et al. (2005) for the full description on the IAGCs.

suspected as the foreground dwarfs (small circles in our plots)<sup>14</sup>. Seventeen are left as bona fide old M31 GCs (see also Beasley et al. 2005). In our plots, however, we have depicted the genuine old M31 GCs with high S/N ( $\geq 60$ ) using bigger asterisks<sup>15</sup> compared to the ones with low S/N (smaller asterisks)<sup>16</sup>. Our plots are drawn mainly in Mg  $b$  vs. Lick indices planes so that not only could we take advantage of one of the most  $\alpha$ -sensitive index (Mg  $b$ ) but some direct comparisons with Fig. 2 of TMB03a are possible.

Our models in Figures 7–9 are the same as those in Figures 1 and 2. From Figures 7–9, the following is noted: (1) in general, our models satisfactorily match M31 GCs as well as Milky Way GCs at 12 Gyr *without zero-point shifts* which Thomas, Maraston, & Korn (2004; hereafter TMK04) models notably needed (see Beasley et al. (2005)’s Figs. 3, 4, 5), (2) The YSCs are consistently located around the 1 Gyr line, (3) The IAGCs are well-separated from the genuine old M31 GCs in the  $H\beta$  diagram. In the  $H\gamma_A$  diagram, they may overlap with old clusters. At  $H\gamma_A$  and  $H\delta_A$ , the IAGCs look  $\sim 3$ – $5$  Gyr old, but they appear  $\sim 2$ – $5$  Gyr old from  $H\beta$ . The  $[\text{Fe}/\text{H}]$  of the IAGCs is confined between  $-1.0$  and  $-0.5$ .

We predict that if the IAGCs are truly intermediate-age ( $\sim 2$ – $5$  Gyr) instead of old-age ( $\sim 12$  Gyr) then they should NOT be detected with the GALEX far-UV photometry (see Fig. 2 of Lee et al. 2003). This also has implications for other suggested intermediate-age star clusters found among interacting galaxies (e.g., Goudfrooij et al. 2001). In this respect, it is very interesting to note that one M31 GC in particular, 311-033, has an age estimated at about 5 Gyr by Burstein et al. (2004) from its integrated spectra, but a recent HST CMD by Rich et al. (2005) clearly shows that this globular cluster has a well-developed blue horizontal-branch.

Figures 10–12 show non-Balmer indices. In all diagrams we note that old M31 GCs mostly overlap with Milky Way GCs. Also, from the comparison with the two most metal-rich Milky Way GCs, NGC 6553 and NGC 6528, it seems that there is no super-solar metallicity M31 GC among Beasley et al. sample. In fact, the most metal-rich M31 GC from the Beasley et al. sample looks similar to the Galactic GCs NGC 6528 and NGC 6553 in Mg  $b$  and it is 163-217 (small asterisk). Overall, the metallicity range of M31 globular clusters is similar to that of their Galactic counterparts, within sample selection effects and small number statistics. It is further noted that the YSCs stand out in the moderately age-sensitive CN and G4300 diagrams. Finally, for the purpose of weeding out foreground dwarfs (small circles),  $\text{CN}_1$ ,  $\text{CN}_2$ ,  $\text{Mg}_1$ , Na D, and  $\text{TiO}_1$  look useful. The detailed descriptions of some

---

<sup>14</sup>They are NB 68, NB 74, NB 81, NB 83, NB 87, and NB 91.

<sup>15</sup>They are 134-190, 158-213, 225-280, 234-290, 347-154, 365-284, 383-318, and NB 89.

<sup>16</sup>They are 163-217, 304-028, 310-032, 313-036, 328-054, 350-162, 393-330, 398-341, and 401-344.

notable indices are given below. Although we show YSCs, IAGCs, and dwarfs in our plots, we mainly describe the genuine old M31 GCs because our 12 Gyr models are compared with the data.

$CN_1$ ,  $CN_2$ : The top panels of Figure 10 show that M31 GCs are also systematically stronger than our models both in  $CN_1$  and  $CN_2$  by  $\sim 0.04$  mag similar to Milky Way GCs in Fig. 3<sup>17</sup>.  $G4300$ ,  $C24668$ : The middle panels of Figure 10 illustrate that M31 GCs data nicely overlap with C98 and our models.  $Ca4227$ : It is seen from the bottom left panel of Figure 10 that both the Milky Way and M31 GCs are systematically weaker than our models at the metal-rich ( $[Fe/H] > -0.5$ ) regime.  $Ca4455$ : The bottom right panel of Figure 10 shows that M31 GCs data overlap with C98 rather than P02 Milky Way data, albeit with some systematic offsets from our models.

$Fe4383$ ,  $Fe5270$ ,  $Fe5335$ ,  $Fe5406$ ,  $Fe5709$ ,  $Fe5782$ ,  $Mg_2$ ,  $Fe4531$ : From Figures 11 and 12, it is seen that M31 GCs generally overlap with Milky Way GCs and with our models.  $Fe5015$ : The middle right panel of Figure 12 shows that M31 GCs go well with Milky Way GCs with similar amounts of systematic offset seen in Figure 6.  $Na D$ : The bottom right panel of Figure 12 shows that M31 GCs generally overlap with Milky Way GCs, suggesting some similar Na absorption in interstellar material and/or a possible Na–O anti-correlation among M31 GC stars.  $TiO_1$ : It is seen from the bottom left panel of Figure 12 that M31 GCs mostly overlap with C98, though with some systematic offset ( $\sim 0.01$ – $0.02$  mag) from our models.

### 3.3. COMPARISON WITH EARLY-TYPE GALAXIES

In this section, we investigate the  $\alpha$ -element enhancement phenomena among early-type galaxies, such as the well-known Mg enhancement that have been reported over the last decade (e.g., Worthey et al. 1992). Our primary data set is the Lick/IDS early-type galaxies of Trager et al. (1998). This data set has the advantage that it is on the Lick/IDS index system and that it contains a large number of galaxies. The set has two major disadvantages. First, the observational errors for any single galaxy are large, usually too large to have very useful age or metallicity discrimination. Second, the additional Balmer feature indices of Worthey & Ottaviani (1997) are not included. We gloss over the first problem for this paper by taking median values (really biweight locations; see below) and we fix the second

---

<sup>17</sup>We note that Beasley et al. (2004) and Burstein et al. (2004) recently report that M31 GCs have higher nitrogen abundance compared to Milky Way GCs using near-UV  $CN3883 \text{ \AA}$  and  $NH3360 \text{ \AA}$  features, respectively.

problem by publishing here the H $\gamma$  and H $\delta$  index measurements for almost all of the Trager et al. (1998) sample.

The treatment of the Balmer indices in the Lick/IDS data set proceeds much as outlined in Trager et al. (1998), and we refer readers to that paper for a more detailed explanation. In brief, the program AUTOINDEX, written by Jesús González, was used to measure the index values. This program cross-correlates spectral regions in the immediate neighborhood of the index wavelength definition to refine the wavelength scale before index measurement. Error estimation comes from a ratio of the power in pixel-to-pixel (assumed mostly photon statistics) variations to the total power in the spectrum, where the analysis is done in Fourier-transformed spectra. This  $G$  factor was related to real measurement error by comparing with multiply-observed galaxies and scaled appropriately, as in Trager et al. (1998) section 3.

Velocity dispersion corrections were computed from artificially broadened templates that included G and K stars and low- $\sigma$  galaxies. The  $C_j(\sigma)$  multiplicative corrections are listed here [see Trager et al. (1998) equation 12] as a function of velocity dispersion  $\sigma$ . The Trager et al. (1998) Table 4 velocity dispersions were adopted.

$$C_{\delta A} = 1 - 1.111 \times 10^{-5} \sigma + 9.333 \times 10^{-7} \sigma^2 - 6.914 \times 10^{-10} \sigma^3 \quad (3)$$

$$C_{\gamma A} = 1 - 8.000 \times 10^{-5} \sigma + 4.222 \times 10^{-7} \sigma^2 - 1.482 \times 10^{-10} \sigma^3 \quad (4)$$

$$C_{\delta F} = 1 - 4.556 \times 10^{-5} \sigma - 7.778 \times 10^{-7} \sigma^2 + 9.877 \times 10^{-10} \sigma^3 \quad (5)$$

$$C_{\gamma F} = 1 + 1.667 \times 10^{-5} \sigma + 3.778 \times 10^{-7} \sigma^2 - 5.926 \times 10^{-10} \sigma^3 \quad (6)$$

The velocity dispersion corrections are among the mildest of the Lick/IDS index set. At  $\sigma = 400 \text{ km s}^{-1}$ , the corrections are about 10% for both H $\delta$  indices, and about 2% for both H $\gamma$  indices. Thus, the contribution to the total error from velocity dispersion is almost negligible (although we included it). The error estimation scheme may not work as well for H $\delta$  as for H $\gamma$  because it lies at the blue end of the spectrum, and therefore may suffer from photon noise in a somewhat more nonlinear way than the central portion of the spectrum that was used to calculate the Fourier  $G$  parameter. Nevertheless, we present the index measurements and errors in Table 1 as our current best guess. The overall accuracy of the errors may, as in Trager et al. (1998), be as good as 5% for the H $\gamma$  indices, but we doubt they are quite that good for H $\delta$ .

For purposes of plotting this noisy data set, the galaxy data are binned by velocity dispersion and listed in Table 2. Instead of mean and standard deviation, we derive the more robust Tukey biweight location and scale (Beers, Flynn, & Gebhardt 1990; Tukey 1958). We note that the smaller galaxies are observed to have a much broader intrinsic scatter.

Median measurement error is about the same for the smaller galaxies as for the larger ones, so the increased scatter in small galaxies is intrinsic to the galaxies, not an artifact of photon statistics. The implication is that the driving parameters of the integrated spectrum (age, metallicity, nebular emission) are more varied in the small galaxies compared to the large ones. This agrees with earlier inferences from the same Lick/IDS data set (Worthey 1996, 1998) but also from considerations of the Mg- $\sigma$  diagram (Bender et al. 1993; Worthey & Collobert 2003), where nebular emission is not a factor.

In Figures 13–19, the  $\sigma$ -binned median galaxy indices are depicted as large open squares. In addition to the median data, two individual galaxies with low observational errors, M31 (big open circle on the metal-rich side) and M32 (big open circle on the metal-poor side), are also plotted. Figures 13 and 14 show Balmer index diagrams, while Figures 15–19 show metallic features. What we look into from these plots are the SSP-equivalent ages and metallicities of galaxies because they are generally composed of mixtures of stellar populations with a range of ages and metallicities.

Figure 13 shows a comparison of Lick/IDS early-type galaxies with our models in Mg  $b$  vs.  $H\beta$  (left panel) and in Fe5270 vs.  $H\beta$  (right panel). M31 star clusters of all ages are also plotted. The top pair of panels has  $[\alpha/\text{Fe}] = 0$ , the middle pair of panels has  $[\alpha/\text{Fe}] = +0.3$ , and the bottom pair of panels has  $[\alpha/\text{Fe}] = +0.6$ , applied only at  $[\text{Fe}/\text{H}] = 0.0$  and  $+0.5$  as usual. The high  $\alpha$ -sensitivity of Mg  $b$  (left panel) and the  $\alpha$ -insensitivity of Fe5270 (right panel) are abundantly illustrated. Figure 14 is a clone of Figure 13, except using  $H\gamma_A$  instead of  $H\beta$  in order to show the  $\alpha$ -sensitivity of  $H\gamma_A$ <sup>18</sup>.

As we apply our various  $\alpha$ -enhanced models to the data in Figures 13 and 14, we find that vastly different age,  $[\text{Fe}/\text{H}]$ , and  $[\alpha/\text{Fe}]$  estimation is possible for the early-type galaxies depending upon the selected combination of metal lines and Balmer lines. The well-known Mg enhancement is prominent from upper panels of Figures 13 and 14 as galaxy data are compared with our models from solar-scaled isochrones without HTWB02 treatment. It is seen from middle panels of Figures 13 and 14, however, that our models of  $[\alpha/\text{Fe}] = +0.3$  dex consistently give a similar estimation of age and metallicity both from Mg  $b$  and Fe5270 for high- $\sigma$  galaxies.

The low  $\sigma$  galaxies ( $\sigma < 100$  km/sec) that have the lowest values in Mg  $b$  and Fe5270 have consistent ages only in the  $[\alpha/\text{Fe}]=0$  panels, as one would expect from, e.g. Figure 17. The median low  $\sigma$  galaxy also looks younger than high  $\sigma$  counterparts in Figures 13 and 14

---

<sup>18</sup>All our other models of high-order Balmer line indices ( $H\gamma_F$ ,  $H\delta_A$ , and  $H\delta_F$ ) are also similarly significantly  $\alpha$ -sensitive confirming the previous work of TMK04 (cf., Tantaló & Chiosi 2004). They are available at our website, <http://astro.wsu.edu/hclee/sp.html>.

(see also Caldwell, Rose, & Concannon 2003), but of course the scatter in this bin is larger, so old-and-small galaxies do exist.

We turn now to the metallic indices plotted in Figures 15–19. The Lick IDS early-type galaxies plotted against our models, particularly from Figure 17, show that they are generally of  $-0.5 \leq [\text{Fe}/\text{H}] \leq +0.2$  with  $[\alpha/\text{Fe}] \sim +0.3$  dex. It is also seen from Figure 17 that the  $[\alpha/\text{Fe}]$  of galaxies, at least as traced by Mg and Na, seems to increase with increasing velocity dispersion (Trager et al. 2000b). As Milky Way and bona fide old M31 GCs are compared with Lick/IDS early-type galaxies in Figures 15–19, the following details are also noted.

*Mg*: The well-known Mg enhancement phenomenon of early-type galaxies is again confirmed from our models of Mg *b* vs. Fe4383 in the top left panel of Figure 17 show this issue more clearly, because Mg *b* is strongly  $\alpha$ -sensitive while Fe4383 is  $\alpha$ -anti-sensitive.

*CN<sub>1</sub>, CN<sub>2</sub>*: The top panels of Figure 15 show that Lick/IDS early-type galaxies are systematically of lower values than the Milky Way and M31 GCs both in CN<sub>1</sub> and CN<sub>2</sub> by  $\sim 0.03$ – $0.04$  mag (see also Fig. 3 of Beasley et al. 2004). Assuming no problems with the data, this points out a distinct difference between globular clusters and early-type galaxies. We speculate that the globular cluster environment is perhaps special and different from that of galaxies, and that this is manifested in the CN index strengths either due to N abundance effects, or perhaps a CH-CN bimodality phenomenon. The same behavior is seen in CN diagrams versus Fe indices.

*Ca4227*: As shown in the bottom left panel of Figure 15, all the metal-rich ( $[\text{Fe}/\text{H}] > -0.5$ ) Milky Way and M31 GCs and Lick/IDS early-type galaxies are of systematically lower Ca4227 values compared to our models. The “Ca underabundance” (e.g., TMB03b; Cenarro et al. 2004) of early-type galaxies is manifested here. Figure 16 shows, however, that Ca4227 vs. Fe indices does *not* show any significant under- or over-abundance. That is, in diagrams involving Fe indices, the galaxies follow the scaled-solar models. We tend to agree with Worthey (1998) that while Mg, Na, and perhaps N are enhanced with respect to Fe, Ca is not.

*TiO<sub>1</sub> and TiO<sub>2</sub>*: It is seen from the bottom left panel of Figure 19 that Lick/IDS early-type galaxies overlap and extend the metal-rich end of the Milky Way (C98) and M31 GCs. Curiously, many GCs appear to have much stronger TiO absorption than the most metal-rich of galaxies. Perhaps some stochastic effect can account for this, but our favorite explanation is another appeal to the slippery transformation from CCD to Lick/IDS systems. In this case, the TiO indices are both broad in wavelength and at the red end of the spectrum, both of which leave the index especially sensitive to systematic errors induced by spectrophotometric shape effects.

#### 4. SUMMARY & CONCLUSION

In this study we presented new simple stellar population models that predict 25 Lick IDS index strengths and cover a broad range of age and metallicity. They include  $\alpha$ -element enhancement by virtue of the fact that they are based on the  $\alpha$ -enhanced  $Y^2$  isochrones and HTWB02 response functions for Lick IDS indices. The effects from horizontal-branch stars are fully incorporated.

Among Balmer lines, a significant  $\alpha$ -enhancement effect was noted for  $H\gamma$  and  $H\delta$ , but  $H\beta$  is rather  $\alpha$ -insensitive. We also find that our 5 Gyr and 12 Gyr models of  $H\gamma$  and  $H\delta$  overlap at the metal-poor regime because of blue horizontal-branch stars. It is further noted that younger than 1 Gyr and for metal-poor populations, Balmer lines become weaker because the main-sequence turnoff becomes hotter than 10,000 K.

Our  $\alpha$ -enhanced models are presented at fixed  $[\text{Fe}/\text{H}]$ , therefore making it straightforward to test our models using Milky Way globular clusters that have independently-estimated mean  $[\text{Fe}/\text{H}]$  and  $[\alpha/\text{Fe}]$ . At the solar and super-solar metallicity end, we have further employed the updated Lick IDS index response functions by HTWB02 so that we could assess element enhancement in early-type galaxies. Our models should be useful for distant unresolved stellar systems in order to extract some useful information on their age, metallicity, and  $\alpha$ -enhancement.

From the comparisons of our models with observations of Milky Way and M31 GCs, we find that our models of Balmer lines satisfactorily trace them at 12 Gyr *without the need for zero-point shifts* which some previous models require. We also verify the plausible existence of young and intermediate-age star clusters in M31 that Beasley et al. (2004, 2005) recently claimed. We derive their ages at around  $\sim 1$  Gyr and  $\sim 2$ –5 Gyr, respectively, from our models. We predict that these latter ones are truly intermediate-age ( $\sim 2$ –5 Gyr) instead of old-age ( $\sim 12$  Gyr) if they are *not* detected with GALEX far-UV photometry. We do not find any super-solar metallicity M31 GCs from Beasley et al. (2004)’s sample. The metallicity range of M31 GCs in Beasley et al. (2004) is similar to that of their Galactic counterparts. Contrary to the literature values, the Milky Way GC NGC 6553 appears slightly more metal-rich than NGC 6528 based on the strength of their metal indices.

We confirm and understand the well-known Mg enhancement phenomenon among metal-rich early-type galaxies. Our models with  $[\alpha/\text{Fe}] = +0.3$  dex consistently provide similar estimation of age and metallicity both from Mg and Fe indices. Also, it is noted that  $[\alpha/\text{Fe}]$  of galaxies, as traced by Mg and Na indices, seems to increase with increasing velocity dispersion (but Ca tracks Fe). Moreover, and independent of models, GCs and galaxies follow different tracks in diagrams involving  $\text{CN}_1$  and  $\text{CN}_2$ . This may be telling us something

about N abundance or CH-CN bimodality that is generically different in the globular cluster environment as opposed to the elliptical galaxy environment. It is tempting to speculate that either the extremely high stellar density in globular clusters or some type of partial self-enrichment in globular clusters is the physical driver behind this intriguing difference. Finally, we stress that it is of considerable importance to use these  $\alpha$ -enhanced Lick indices in order to properly assess the mean age and chemical compositions of early-type galaxies.

It is a great pleasure to thank Brad Gibson, Michael Beasley, Rob Proctor, Ricardo Schiavon, Daniel Thomas, Claudia Maraston, and Markus Kissler-Patig for many helpful discussions. We thank Sukyoung Yi for providing us the mass loss table for the  $\alpha$ -enhanced  $Y^2$  isochrones. We also thank an anonymous referee for her/his perspicacious reading of the manuscript which improved this paper significantly. Support for this work was provided by the NSF # 0307487.

## REFERENCES

- Barbuy, B., et al. 2004, *MmSAI*, 75, 398
- Beasley, M. A., Brodie, J. P., Strader, J., Forbes, D. A., Proctor, R. N., Barmby, P. & Huchra, J. P. 2004, *AJ*, 128, 1623
- Beasley, M. A., Brodie, J. P., Strader, J., Forbes, D. A., Proctor, R. N., Barmby, P. & Huchra, J. P. 2005, *AJ*, 129, 1412
- Beers, T. C., Flynn, K., & Gebhardt, K. 1990, *AJ*, 100, 32
- Bender, R., Burstein, R., & Faber, S. M. 1993, *ApJ*, 411, 153
- Burstein, D., Faber, S. M., Gaskell, C. M., & Krumm, N. 1984, *ApJ*, 287, 586
- Burstein, D., et al. 2004, *ApJ*, 614, 158
- Caldwell, N., Rose, J. A., & Concannon, K. D. 2003, *AJ*, 125, 2891
- Cannon, R. D., et al. 1998, *MNRAS*, 298, 601
- Carney, B. W. 1996, *PASP*, 108, 900
- Cenarro, A. J., Sánchez-Blázquez, P., Cardiel, N., & Gorgas, J. 2004, *ApJ*, 614, L101
- Cohen, J. G., Blakeslee, J. P., & Ryzhov, A. 1998, *ApJ*, 496, 808 (C98)

Table 1. Balmer Indices for Lick/IDS Galaxies

Object	$H\delta_A$	$\sigma_{H\delta A}$	$H\gamma_A$	$\sigma_{H\gamma A}$	$H\delta_F$	$\sigma_{H\delta F}$	$H\gamma_F$	$\sigma_{H\gamma F}$
A 569A	-2.596	1.322	-4.961	0.810	-0.178	0.508	-1.326	0.460
IC 171	-2.017	2.215	-5.731	1.371	-0.506	0.874	-1.123	0.772
IC 179	-3.214	1.704	-5.654	1.046	-1.263	0.669	-1.665	0.593
IC 310	-0.176	1.355	-3.612	0.830	0.779	0.525	-1.324	0.472
IC 1696	-1.466	1.251	-5.260	0.776	0.945	0.499	-0.777	0.437
IC 1907	-2.842	1.972	-5.305	1.206	-0.987	0.760	-1.048	0.680
IC 2955	-2.277	1.372	-7.964	0.848	0.064	0.538	-2.808	0.488
IC 4051	-2.311	2.604	-4.136	1.598	-0.010	1.003	-0.813	0.900
NGC 80	-3.224	2.006	-5.068	1.209	-0.293	0.739	-1.626	0.687
NGC 83	-1.130	2.055	-3.526	1.253	-0.067	0.778	-1.916	0.713
NGC 128	...	...	-5.698	0.888	0.010	0.562	-1.470	0.503
NGC 194	-1.074	1.108	-4.709	0.682	0.154	0.431	-0.923	0.386
NGC 205	6.707	1.178	4.951	0.739	4.728	0.498	4.621	0.419
NGC 221	-1.138	0.264	-4.341	0.166	0.669	0.109	-0.416	0.093
NGC 224	-2.514	0.276	-6.405	0.167	-0.027	0.106	-1.394	0.107
NGC 227	-0.854	1.112	-6.562	0.677	0.715	0.427	-2.244	0.403
NGC 315	-2.909	2.305	-6.544	1.375	1.080	0.841	-2.967	0.802

Note. — Table 1 appears in its entirety in the electronic edition of the *Astrophysical Journal Supplement Series*.

Table 2.a. Biweight Locations and Scales for the Lick/IDS Galaxies, Binned by Velocity Dispersion<sup>a</sup>

LOSVD km s <sup>-1</sup>	CN <sub>1</sub>	CN <sub>2</sub>	Ca4227	G4300	Fe4383	Ca4455	Fe4531	C <sub>2</sub> 4668	H $\beta$	Fe5015	Mg <sub>1</sub>	Mg <sub>2</sub>	Mg <i>b</i>
< 100	-0.022	0.030	0.880	4.208	3.905	1.375	2.991	5.089	2.204	4.852	0.068	0.196	3.021
	0.071	0.063	0.505	2.080	1.704	0.495	0.936	2.552	0.802	1.087	0.043	0.067	1.094
	29	29	29	27	29	29	29	29	26	25	27	27	29
100 — 150	0.047	0.082	1.024	5.096	4.733	1.576	3.435	6.481	1.687	4.975	0.112	0.255	4.012
	0.048	0.048	0.308	0.941	0.999	0.333	0.464	1.400	0.561	0.872	0.028	0.042	0.523
	47	47	47	45	47	47	47	47	46	44	47	47	47
150 — 200	0.090	0.125	1.207	5.437	5.121	1.711	3.644	7.449	1.585	5.532	0.140	0.290	4.465
	0.042	0.047	0.449	0.924	1.081	0.410	0.675	1.463	0.463	0.712	0.025	0.033	0.575
	86	86	86	83	86	86	86	86	82	80	86	86	85
200 — 240	0.106	0.147	1.312	5.548	5.298	1.742	3.674	7.871	1.427	5.415	0.152	0.307	4.799
	0.033	0.037	0.437	0.854	0.845	0.362	0.681	1.176	0.446	1.038	0.019	0.027	0.477
	80	80	81	78	81	81	81	81	80	79	80	80	80
240 — 280	0.110	0.151	1.395	5.456	5.244	1.781	3.672	8.078	1.420	5.451	0.160	0.317	4.963
	0.035	0.040	0.366	0.867	0.916	0.372	0.614	1.177	0.414	1.226	0.018	0.022	0.409
	71	71	68	71	71	71	71	71	69	68	70	70	70
> 280	0.134	0.173	1.374	5.388	5.297	1.846	3.915	8.621	1.393	5.550	0.169	0.332	5.127
	0.027	0.031	0.500	0.899	1.013	0.489	0.727	1.314	0.540	1.061	0.017	0.021	0.392
	42	42	42	42	42	42	42	42	41	41	41	41	42

Table 2.b.

LOSVD km s <sup>-1</sup>	Fe5270	Fe5335	Fe5406	Fe5709	Fe5782	Na D	TiO <sub>1</sub>	TiO <sub>2</sub>	H $\delta$ <sub>A</sub>	H $\gamma$ <sub>A</sub>	H $\delta$ <sub>F</sub>	H $\gamma$ <sub>F</sub>
< 100	2.517	2.187	1.485	0.935	0.682	2.952	0.034	0.059	0.698	-3.227	1.481	-0.436
	0.641	0.601	0.492	0.423	0.300	0.790	0.011	0.019	3.263	4.369	1.669	2.436
	29	29	27	25	24	28	29	20	29	27	29	29
100 — 150	2.863	2.452	1.716	0.992	0.794	3.579	0.038	0.079	-1.205	-5.260	0.450	-1.516
	0.437	0.418	0.313	0.228	0.279	0.792	0.011	0.016	1.553	1.894	0.757	1.176
	47	47	45	45	45	47	47	28	45	45	46	46
150 — 200	3.045	2.785	1.925	1.009	0.852	4.575	0.039	0.096	-2.153	-6.103	0.206	-1.917
	0.384	0.426	0.371	0.236	0.320	0.812	0.013	0.013	1.129	1.178	0.714	0.760
	85	83	76	71	81	86	86	44	82	80	85	86
200 — 240	3.107	2.795	1.945	0.977	0.862	4.942	0.041	0.100	-2.344	-6.154	-0.017	-1.951
	0.375	0.440	0.398	0.280	0.335	0.760	0.011	0.010	1.105	1.260	0.640	0.780
	79	79	76	69	79	81	81	30	80	75	80	81
240 — 280	3.018	2.687	1.983	0.965	0.827	5.192	0.045	0.098	-2.359	-6.317	0.013	-1.952
	0.417	0.475	0.367	0.302	0.258	0.703	0.011	0.014	1.057	1.076	0.518	0.566
	70	66	67	64	70	71	71	19	70	70	70	70
> 280	3.230	2.712	1.940	0.883	0.911	5.718	0.045	0.095	-2.860	-6.413	-0.146	-2.112
	0.557	0.580	0.422	0.333	0.424	0.582	0.013	0.016	0.763	0.866	0.557	0.472
	42	41	39	36	40	42	42	8	41	42	42	42

<sup>a</sup>Table is arranged in trios of rows. The first row is the biweight location (median), the second is the biweight scale, a measure of the scatter that is equivalent to a Gaussian  $\sigma$  for Gaussian-distributed data, and the third is the number of galaxies used in the biweight computation for each velocity dispersion bin and index. “LOSVD” is line of sight velocity dispersion.

- Gibson, B. K., Madgwick, D. S., Jones, L. A., Da Costa, G. S., & Norris, J. E. 1999, *AJ*, 118, 1268
- Gibson, B. K., Fenner, Y., Renda, A., Kawata, D., & Lee, H.-c. 2003, *PASA*, 20, 401
- Goudfrooij, P., Mack, J., Kissler-Patig, M., Meylan, G., & Minniti, D. 2001, *MNRAS*, 322, 643
- Gratton, R., et al. 2001, *A&A*, 369, 87
- Harbeck, D., Smith, G. H., & Grebel, E. K. 2003, *AJ*, 125, 197
- Harris, W. E. 1996, *AJ*, 112, 1487
- Houdashelt, M. L., Trager, S. C., Worthey, G., & Bell, R. A. 2002, *BAAS*, 34, 1118 (HTWB02)
- Kim, Y.-C., Demarque, P., Yi, S. K., & Alexander, D. R. 2002, *ApJS*, 143, 499
- Langer, G. E., Suntzeff, N. B., & Kraft, R. P. 1992, *PASP*, 104, 523
- Lee, H.-c., Yoon, S.-J., & Lee, Y.-W. 2000, *AJ*, 120, 998
- Lee, H.-c., Lee, Y.-W., & Gibson, B. K. 2002, *AJ*, 124, 2664
- Lee, H.-c., Lee, Y.-W., & Gibson, B. K. 2003, *Extragalactic Globular Cluster Systems*, ed. M. Kissler-Patig, 261
- Lee, Y.-W., Demarque, P., & Zinn, R. 1994, *ApJ*, 423, 248
- Lejeune, T., Cuisinier, F., & Buser, R. 1997, *A&AS*, 125, 229
- Lejeune, T., Cuisinier, F., & Buser, R. 1998, *A&AS*, 130, 65
- Maraston, C. et al. 2003, *A&A*, 400, 823
- Puzia, T. H., et al. 2002, *A&A*, 395, 45 (P02)
- Ramírez, S. V., & Cohen, J. G. 2002, *AJ*, 125, 224
- Reimers, D. 1975, *Mém. Roy. Soc. Liège* 6. Ser. 8, 369
- Rich, R. M., et al. 2005, *AJ*, 129, 2670
- Salasnich, B., Girardi, L., Weiss, A., & Chiosi, C. 2000, *A&A*, 361, 1023

- Salpeter, E. E. 1955, *ApJ*, 121, 161
- Tantalo, R., & Chiosi, C. 2004, *MNRAS*, 353, 917
- Thomas, D., & Maraston, C. 2003, *A&A*, 401, 429
- Thomas, D., Maraston, C., & Bender, R. 2003a, *MNRAS*, 339, 897 (TMB03a)
- Thomas, D., Maraston, C., & Bender, R. 2003b, *MNRAS*, 343, 279 (TMB03b)
- Thomas, D., Maraston, C., & Korn, A. 2004, *MNRAS*, 351, L19 (TMK04)
- Trager, S. C., Worthey, G., Faber, S. M., Burstein, D., & Gonzalez, J. J. 1998, *ApJS*, 116, 1
- Trager, S. C., Faber, S. M., Worthey, G., & Gonzalez, J. J. 2000a, *AJ*, 119, 1645
- Trager, S. C., Faber, S. M., Worthey, G., & Gonzalez, J. J. 2000b, *AJ*, 120, 165
- Tripicco, M. J., & Bell, R. A. 1995, *AJ*, 110, 3035 (TB95)
- Tukey, J. W., 1958, *Ann. Math. Stat.*, 29, 614
- Wheeler, J. C., Sneden, C., & Truran, J. W., Jr. 1989, *ARA&A*, 27, 279
- Worthey, G. 1996, in *From Stars to Galaxies: The Impact of Stellar Physics on Galaxy Evolution*, ed. C. Leitherer, U. Fritze-von Alvensleben, & J. Huchra, *ASP Conf. Ser.* 98, 467
- Worthey, G. 1998, *PASP*, 110, 888
- Worthey, G. 2004, *AJ*, 128, 2826
- Worthey, G., & Collobert, M. 2003, *ApJ*, 586, 17
- Worthey, G., Faber, S. M., & González, J. J. 1992, *ApJ*, 398, 69
- Worthey, G., Faber, S. M., González, J. J., & Burstein, D. 1994, *ApJS*, 94, 687
- Worthey, G., & Ottaviani, D. L. 1997, *ApJS*, 111, 377
- Yi, S., Demarque, P., & Kim, Y.-C. 1997, *ApJ*, 482, 677

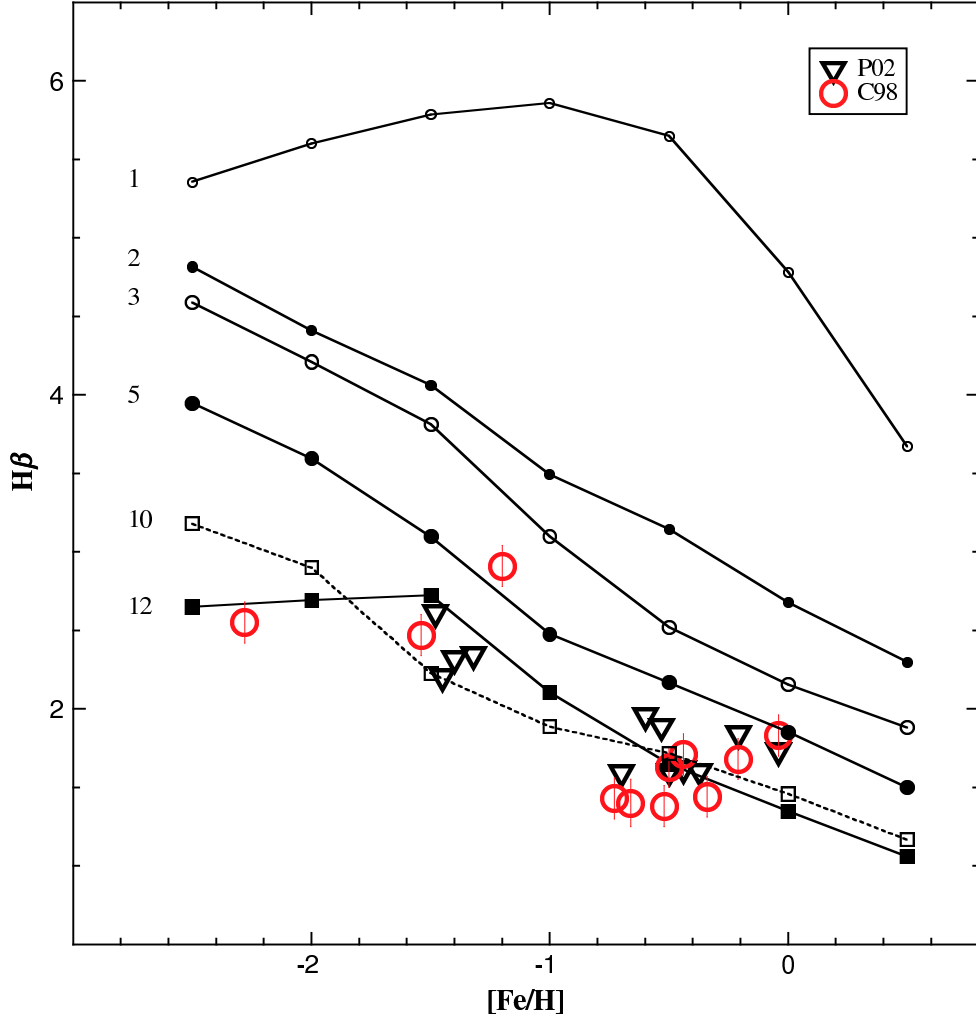


Fig. 1.— Models of  $H\beta$  are compared with Milky Way GCs. Model ages (in Gyr) are indicated on the left. Model points are shown at  $[\text{Fe}/\text{H}] = -2.5, -2.0, -1.5, -1.0, -0.5, 0.0,$  and  $+0.5$ . At  $[\text{Fe}/\text{H}] = 0.0$  and  $+0.5$ , models that incorporate index response functions with  $[\alpha/\text{Fe}] = +0.3$  dex are shown. Cohen et al. (1998; C98, *circles*) and Puzia et al. (2002; P02, *triangles*) observations are overlaid. The  $[\text{Fe}/\text{H}]$  of Milky Way GCs are from Harris (1996). Note that our 12 Gyr models trace the Milky Way GCs without zero-point shifts (see text). The 12 Gyr and 10 Gyr lines cross due to HB morphology effects.

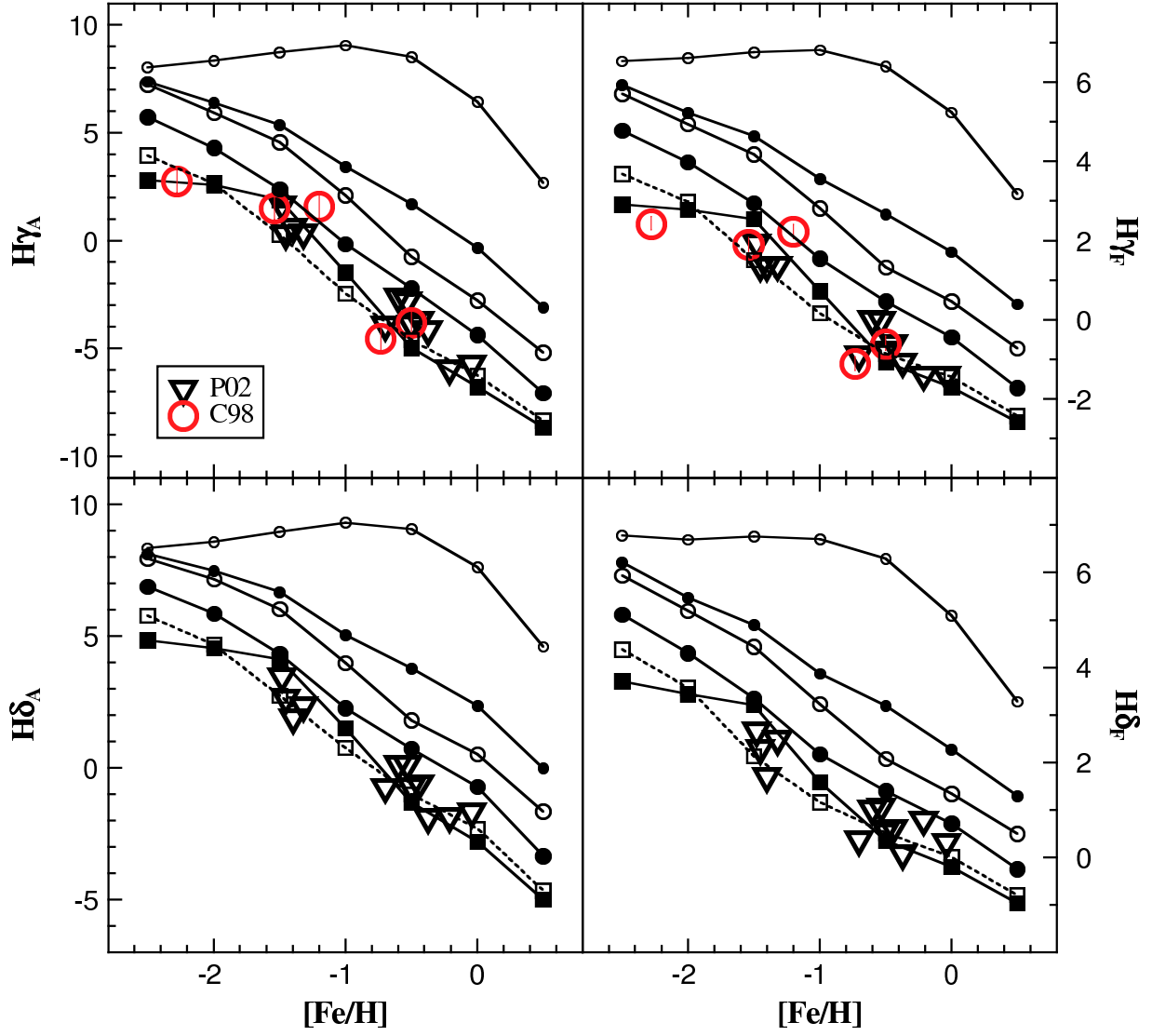


Fig. 2.— Same as Figure 1, but our models of H $\gamma$  and H $\delta$  are compared with Milky Way GCs (see text). Symbols for our models are the same as Figure 1.

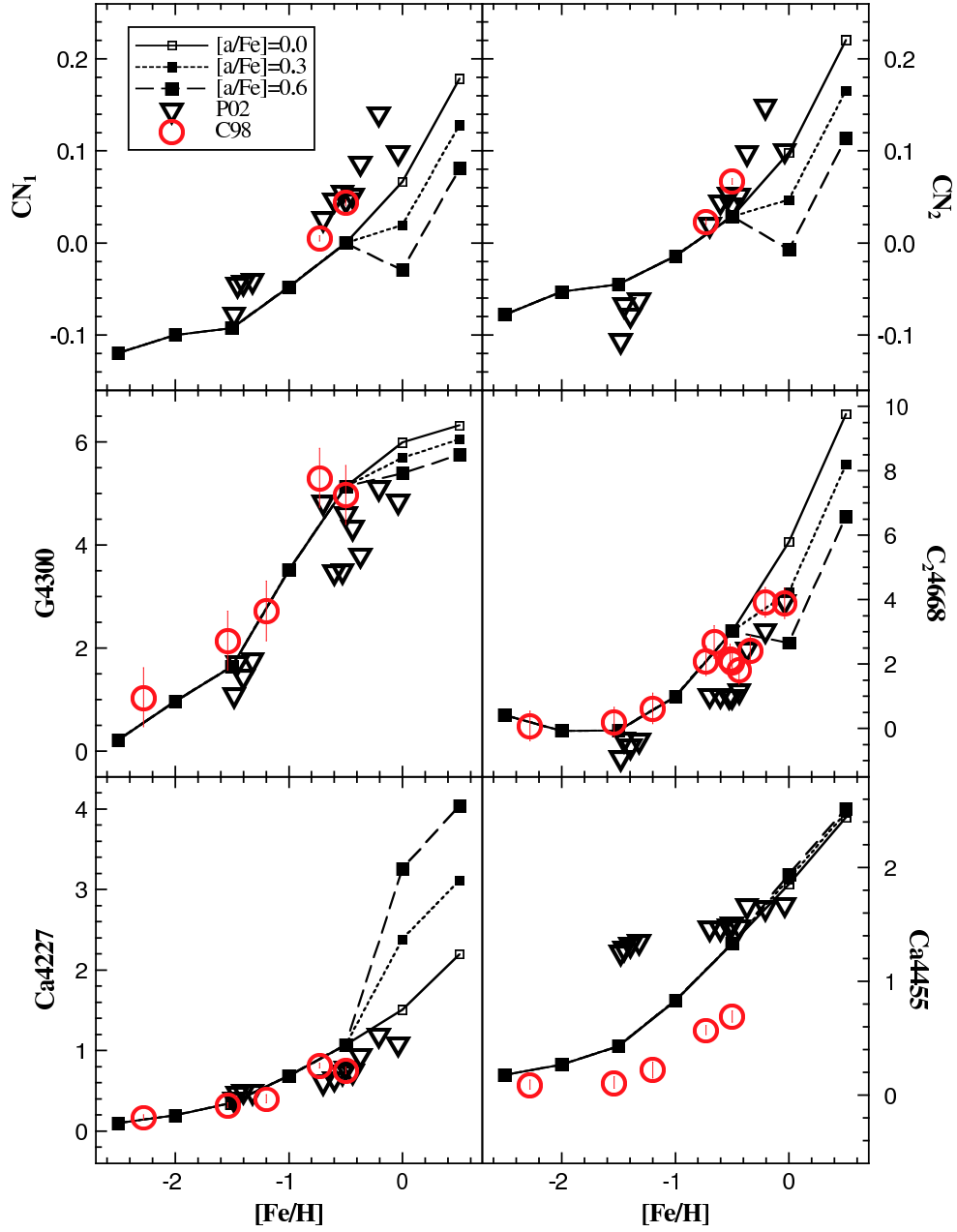


Fig. 3.— 12 Gyr models of  $CN_1$ ,  $CN_2$ , G4300,  $C_24668$ , Ca4227, and Ca4455 are compared with Milky Way GCs. For models of  $[Fe/H] = -2.5, -2.0, -1.5,$  and  $-1.0$ ,  $Y^2$  isochrones with  $[\alpha/Fe] = +0.3$  dex are used. For  $[Fe/H] = -0.5$ ,  $Y^2$  isochrones with  $[\alpha/Fe] = +0.15$  dex are employed. For those of  $[Fe/H] = 0.0$  and  $+0.5$ , solar-scaled  $Y^2$  isochrones are used (*solid lines*) and HTWB02 response functions with  $[\alpha/Fe] = +0.3$  dex (*dotted lines*) and  $+0.6$  dex (*dashed lines*) are applied.

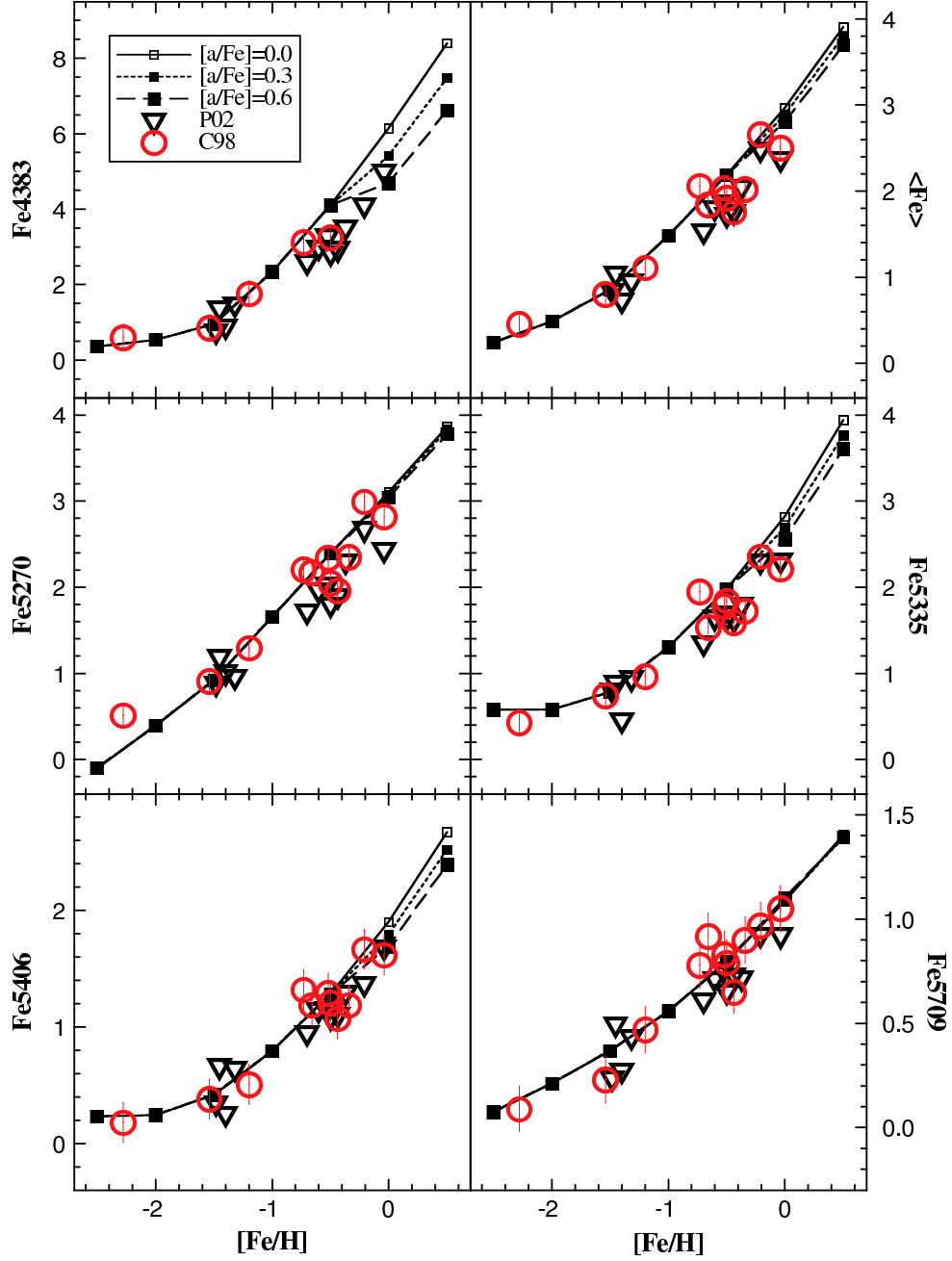


Fig. 4.— Same as Figure 3, but for different indices. 12 Gyr models of Fe4383,  $\langle \text{Fe} \rangle$ , Fe5270, Fe5335, Fe5406, and Fe5709 are compared with Milky Way GCs. Symbols are the same as Figure 3.

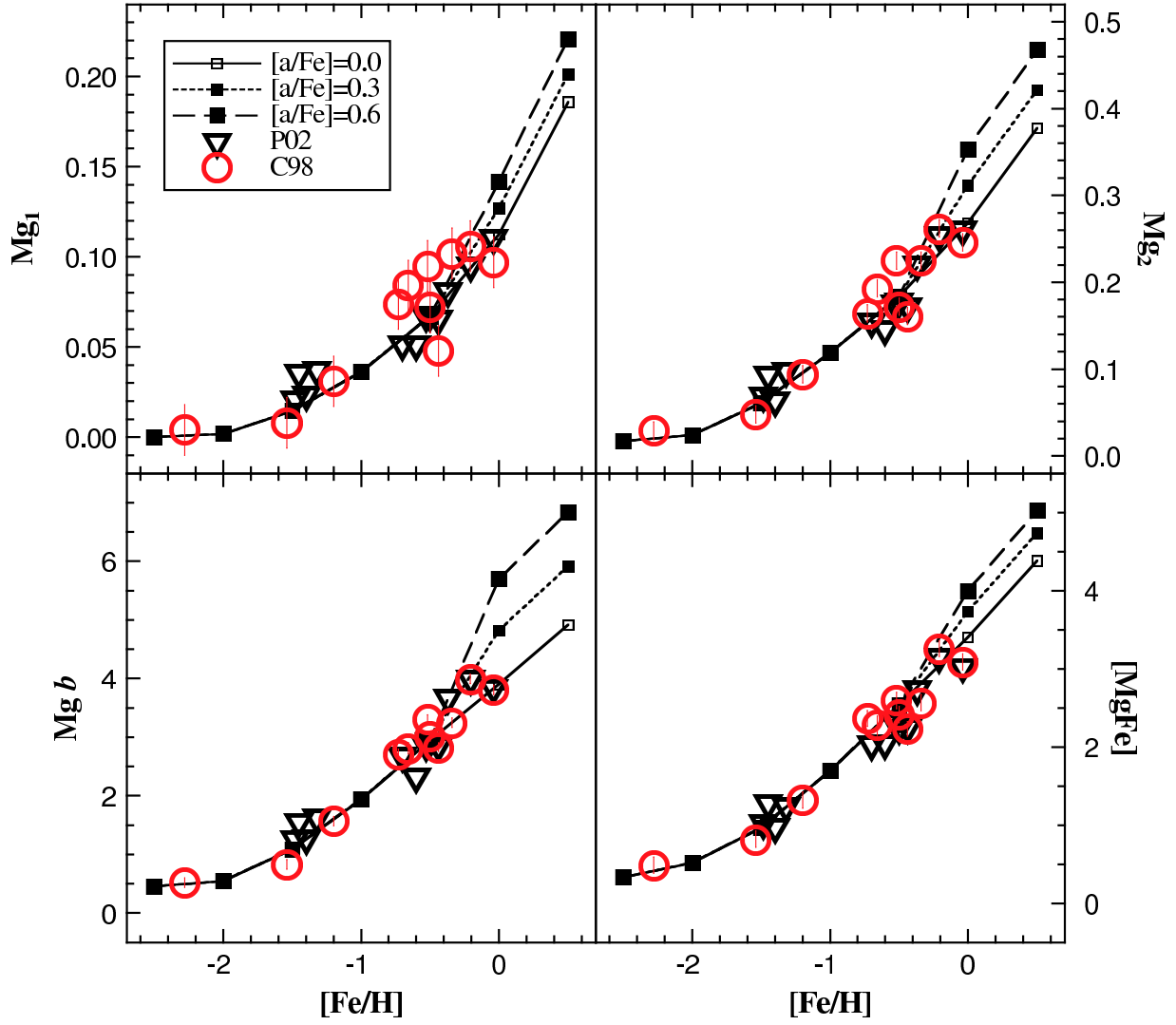


Fig. 5.— Same as Figure 3, but for different indices. 12 Gyr models of  $Mg_1$ ,  $Mg_2$ ,  $Mg\ b$ , and  $[MgFe]$  are compared with Milky Way GCs. Symbols are the same as Figure 3.

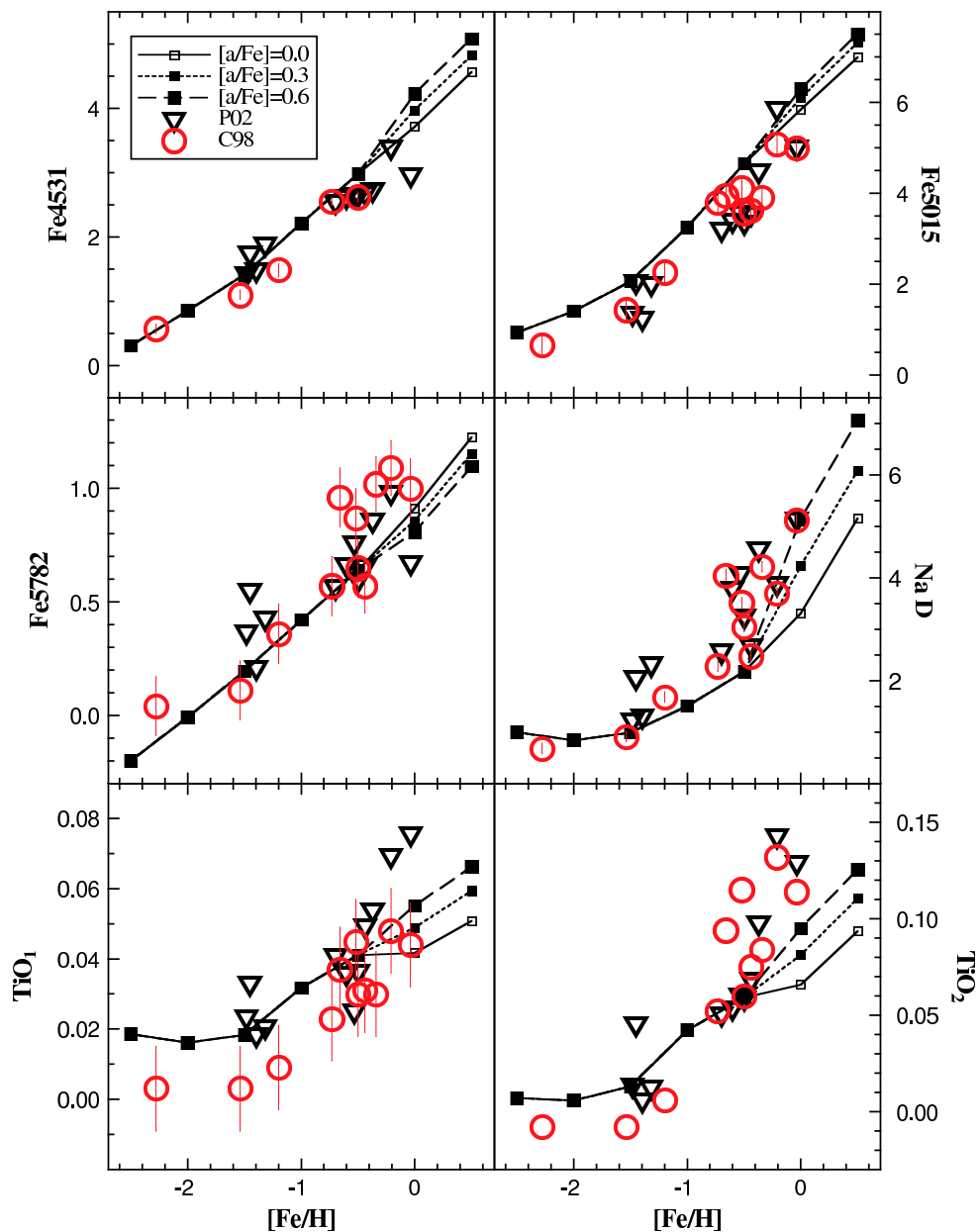


Fig. 6.— Same as Figure 3, but for different indices. 12 Gyr models of Fe4531, Fe5015, Fe5782, Na D, TiO<sub>1</sub>, and TiO<sub>2</sub> are compared with Milky Way GCs. Symbols are the same as Figure 3.

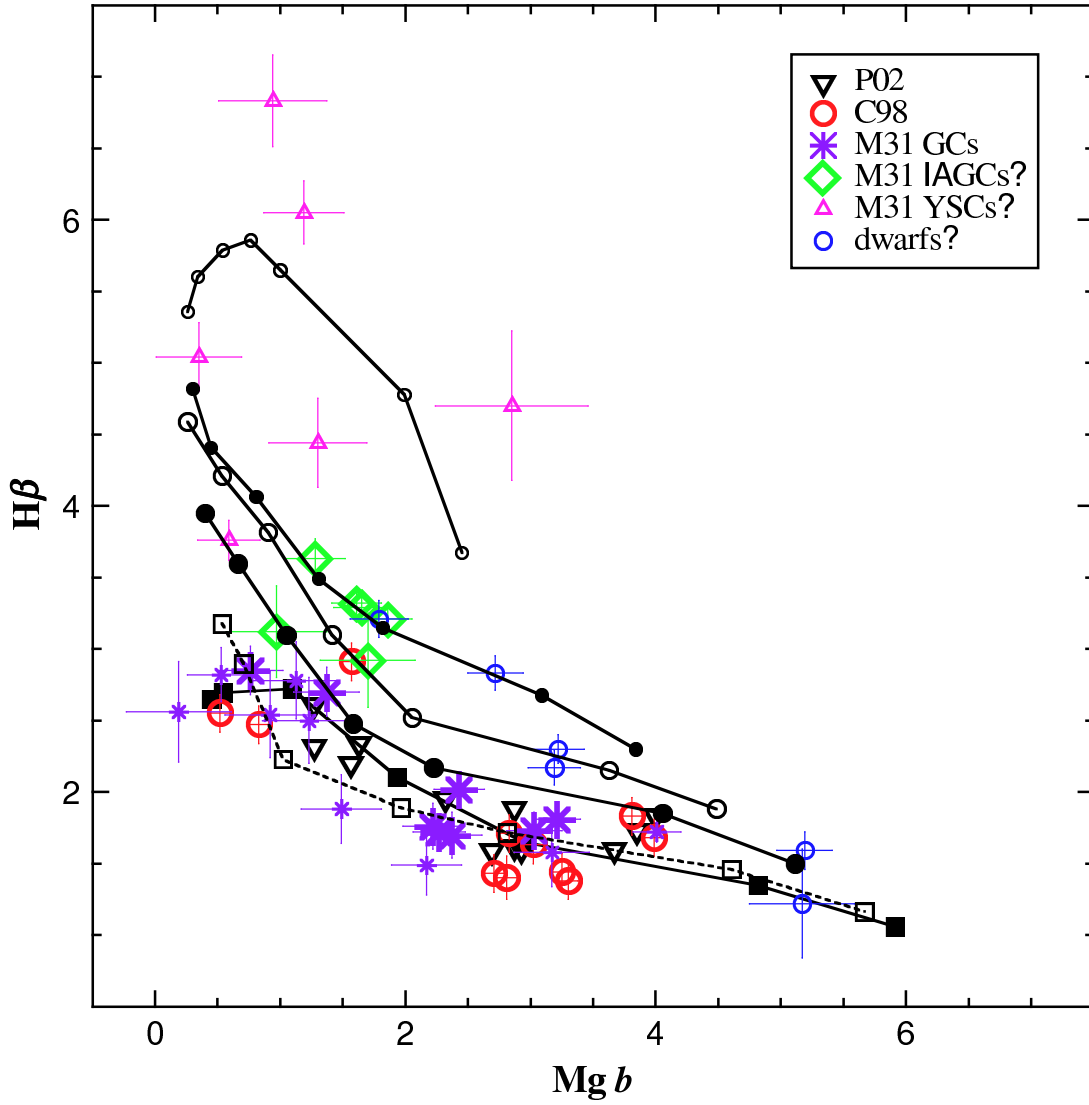


Fig. 7.— Beasley et al. (2004) M31 star clusters are compared with Milky Way GCs and with our models in  $Mg\ b$  vs.  $H\beta$ . Symbols for our models and Milky Way GCs are the same as Figure 1. Bona fide M31 GCs (*asterisks*), bona fide M31 GCs with  $S/N \geq 60$  (*bigger asterisks*), suspected IAGCs (*diamonds*), YSCs (*triangles*), and foreground dwarf stars (*small circles*) are also plotted.

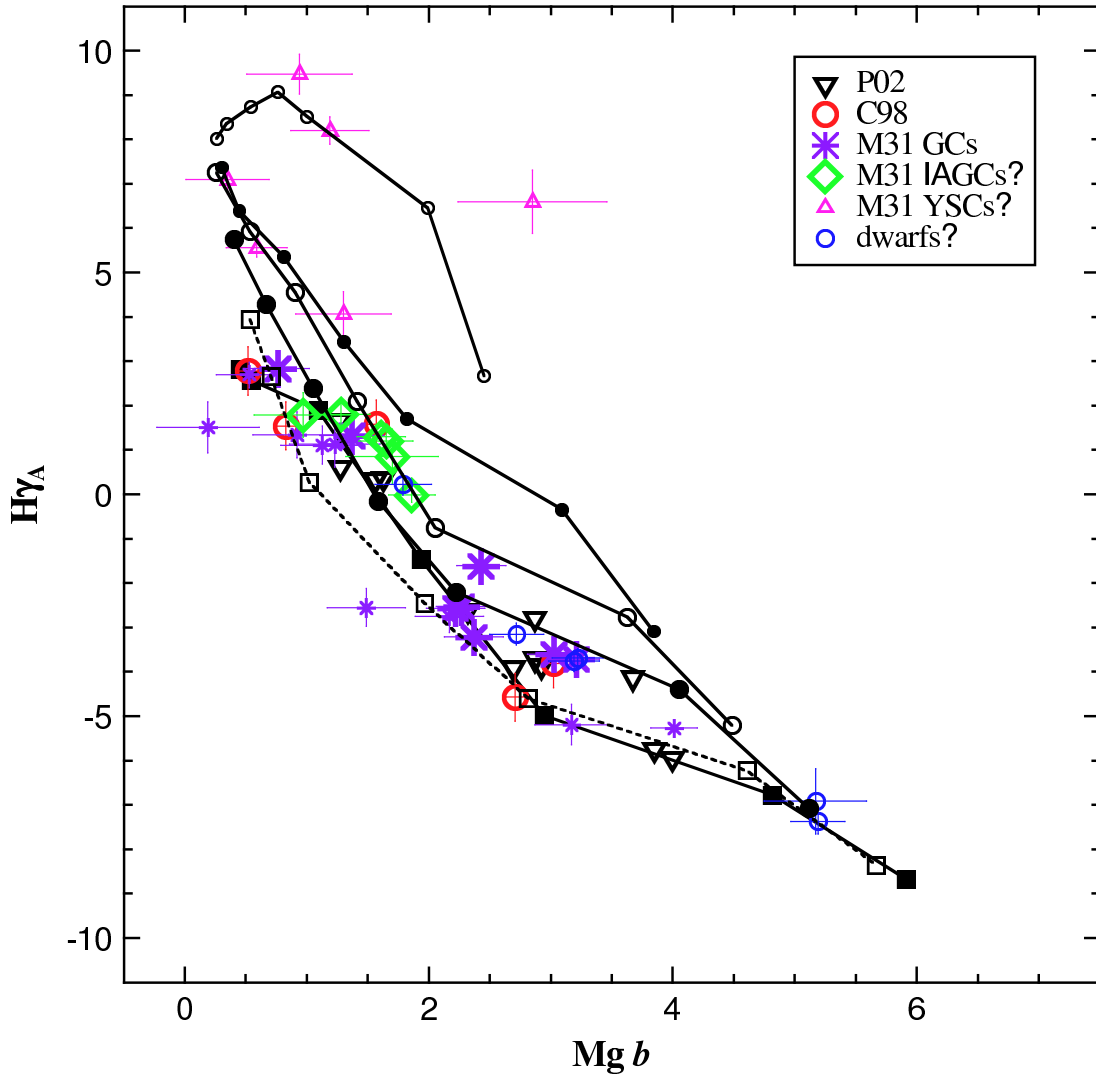


Fig. 8.— Same as Figure 7, but with  $Mg\ b$  vs.  $H\gamma_A$ .

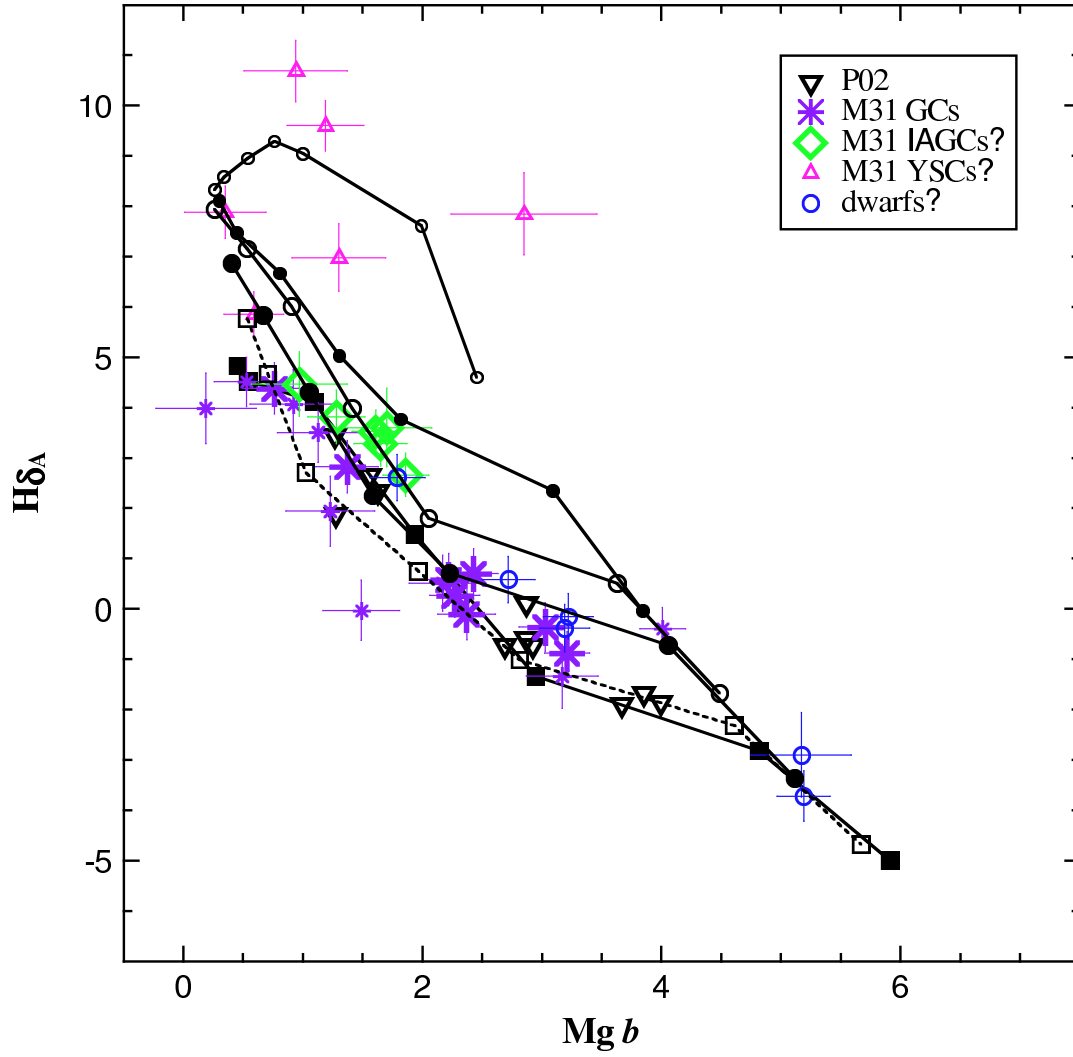


Fig. 9.— Same as Figure 7, but with  $Mg\ b$  vs.  $H\delta_A$ .

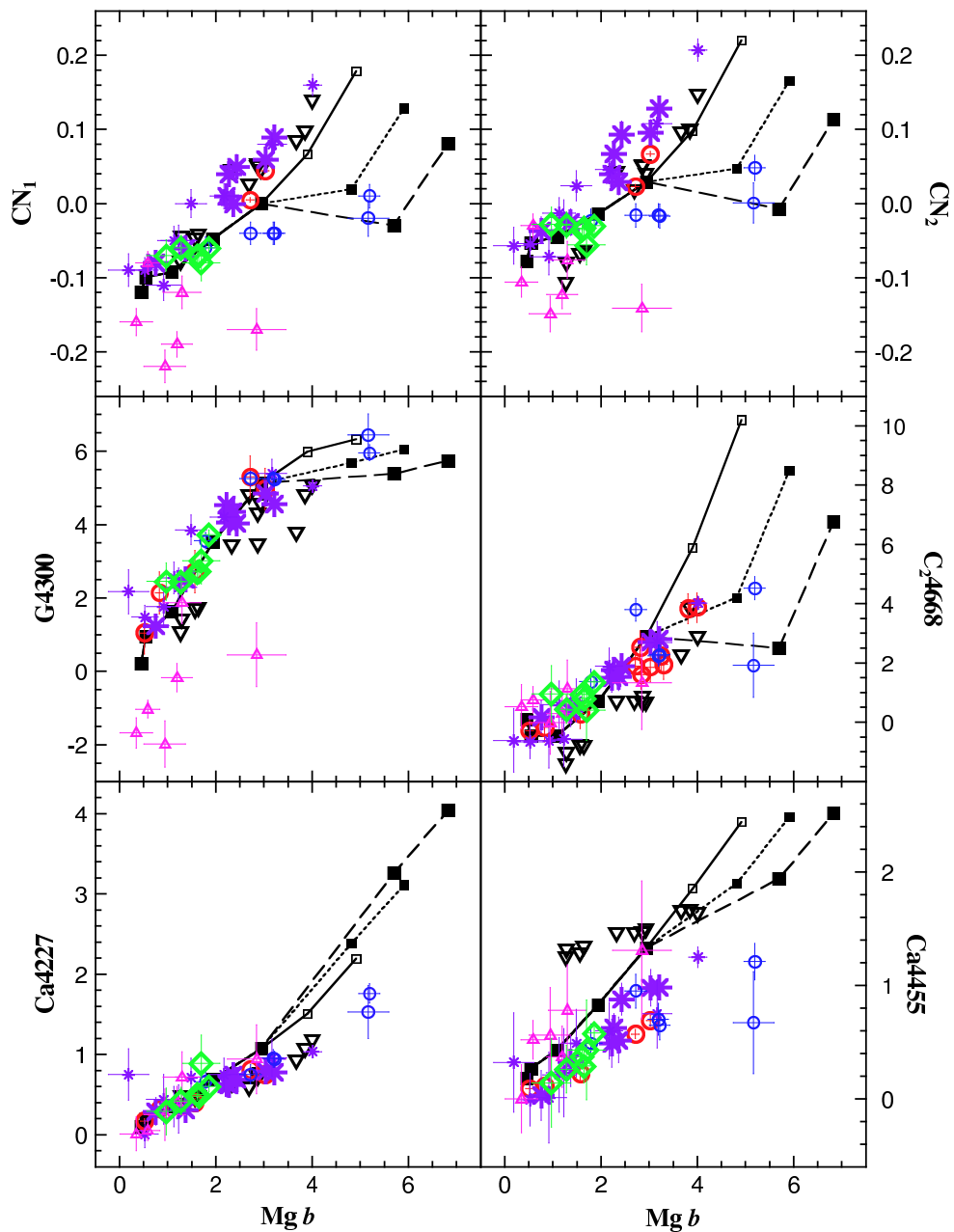


Fig. 10.— Index-index diagrams Similar to Figure 3. M31 star clusters are compared with Milky Way GCs and 12 Gyr models for  $Mg\ b$  vs.  $CN_1$ ,  $CN_2$ ,  $G_{4300}$ ,  $C_{24668}$ ,  $Ca_{4227}$ , and  $Ca_{4455}$ . Symbols are the same as in Figures 3 and 7.

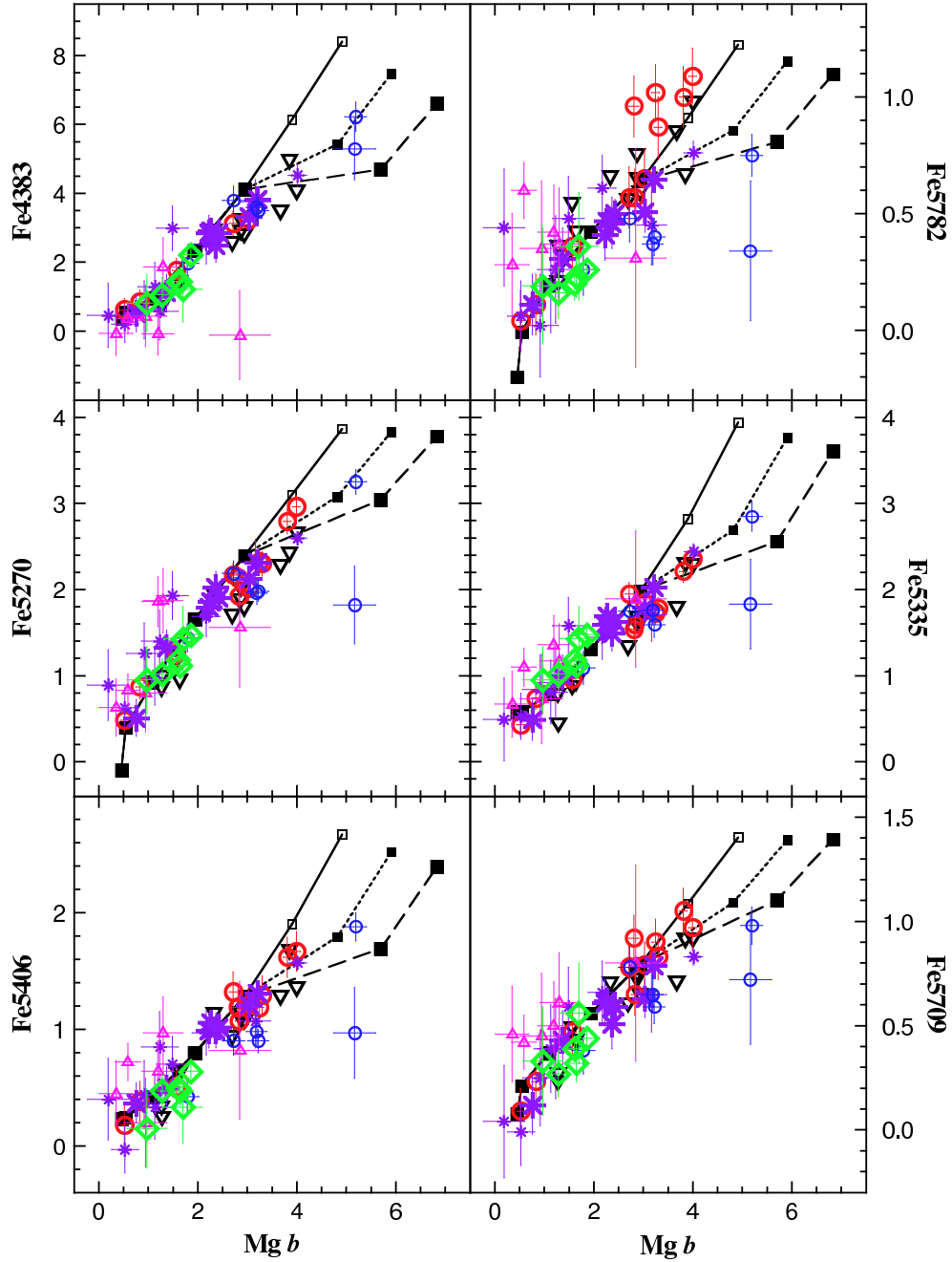


Fig. 11.— Index-index diagrams similar to Figure 4. M31 star clusters are compared with Milky Way GCs and 12 Gyr models for  $Mg\ b$  vs.  $Fe4383$ ,  $Fe5782$ ,  $Fe5270$ ,  $Fe5335$ ,  $Fe5406$ , and  $Fe5709$ . Symbols are the same as in Figures 3 and 7.

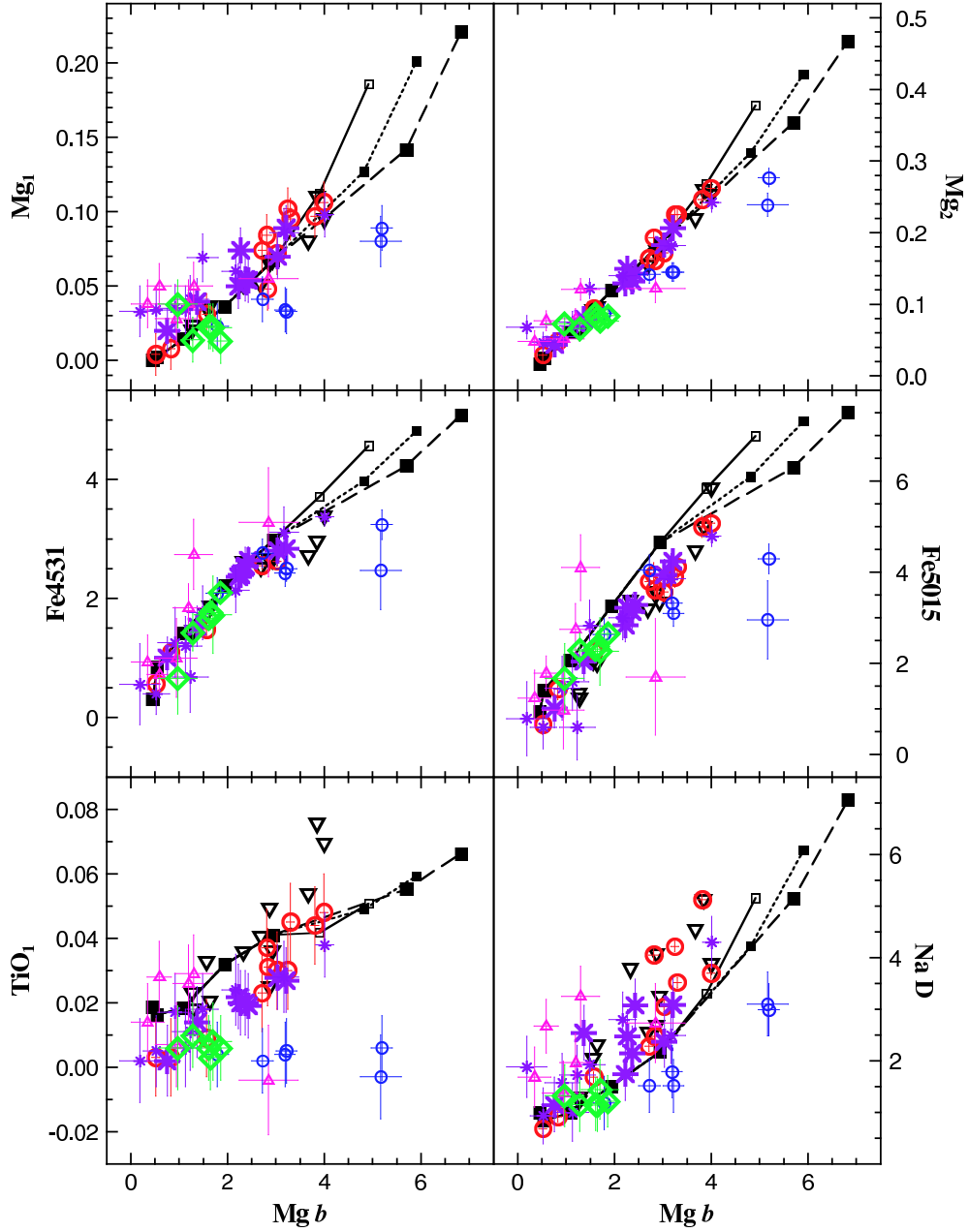


Fig. 12.— Index-index diagrams similar to Figure 6. M31 star clusters are compared with Milky Way GCs and 12 Gyr models for  $Mg\ b$  vs.  $Mg_1$ ,  $Mg_2$ ,  $Fe_{4531}$ ,  $Fe_{5015}$ ,  $TiO_1$ , and  $Na\ D$ . Symbols are the same as Figures 3 and 7.

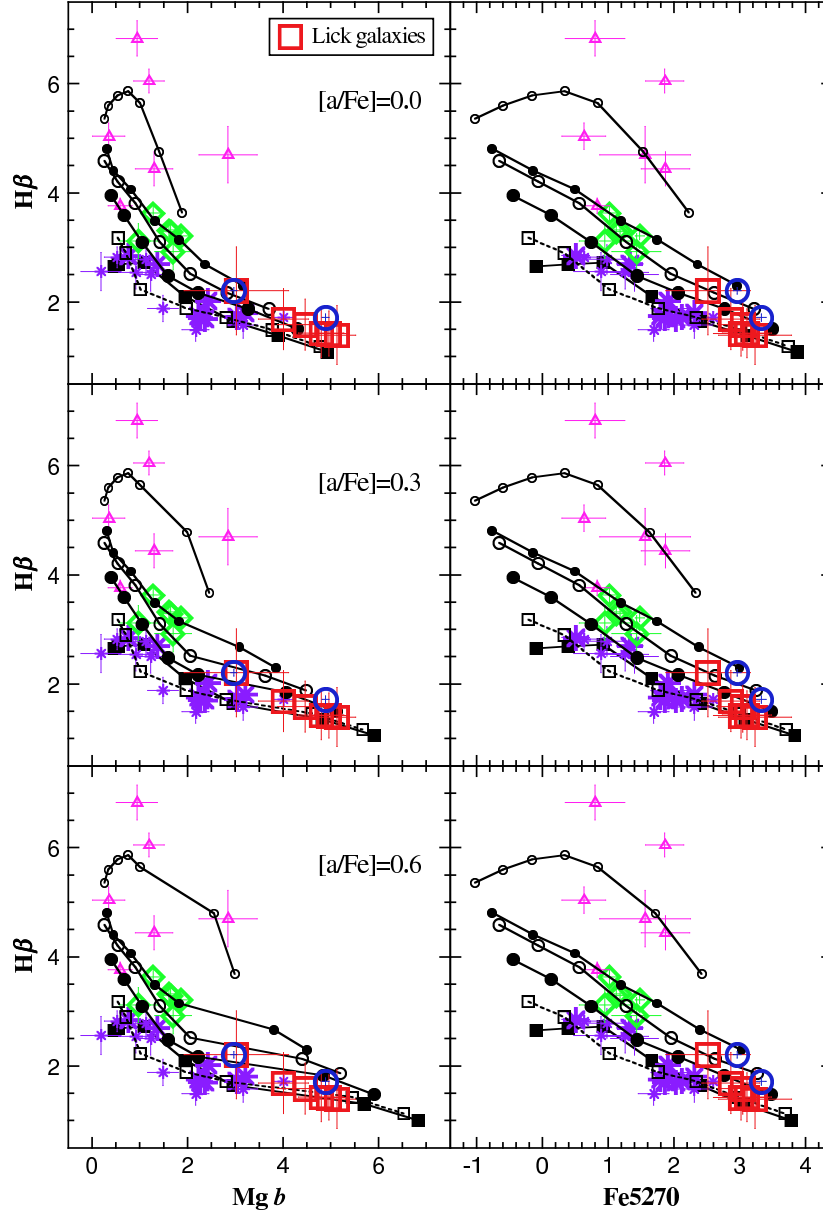


Fig. 13.— Median Lick galaxies (big open squares), M31 (*right big open circle*), and M32 (*left big open circle*) are compared with M31 star clusters (with symbols the same as Figure 7) and with our models in  $Mg\ b$  vs.  $H\beta$  (left panel) and in  $Fe5270$  vs.  $H\beta$  (right panel). At given ages, HTWB02 response functions are applied at  $[Fe/H] = 0.0$  and  $+0.5$  as indicated in the left panels.

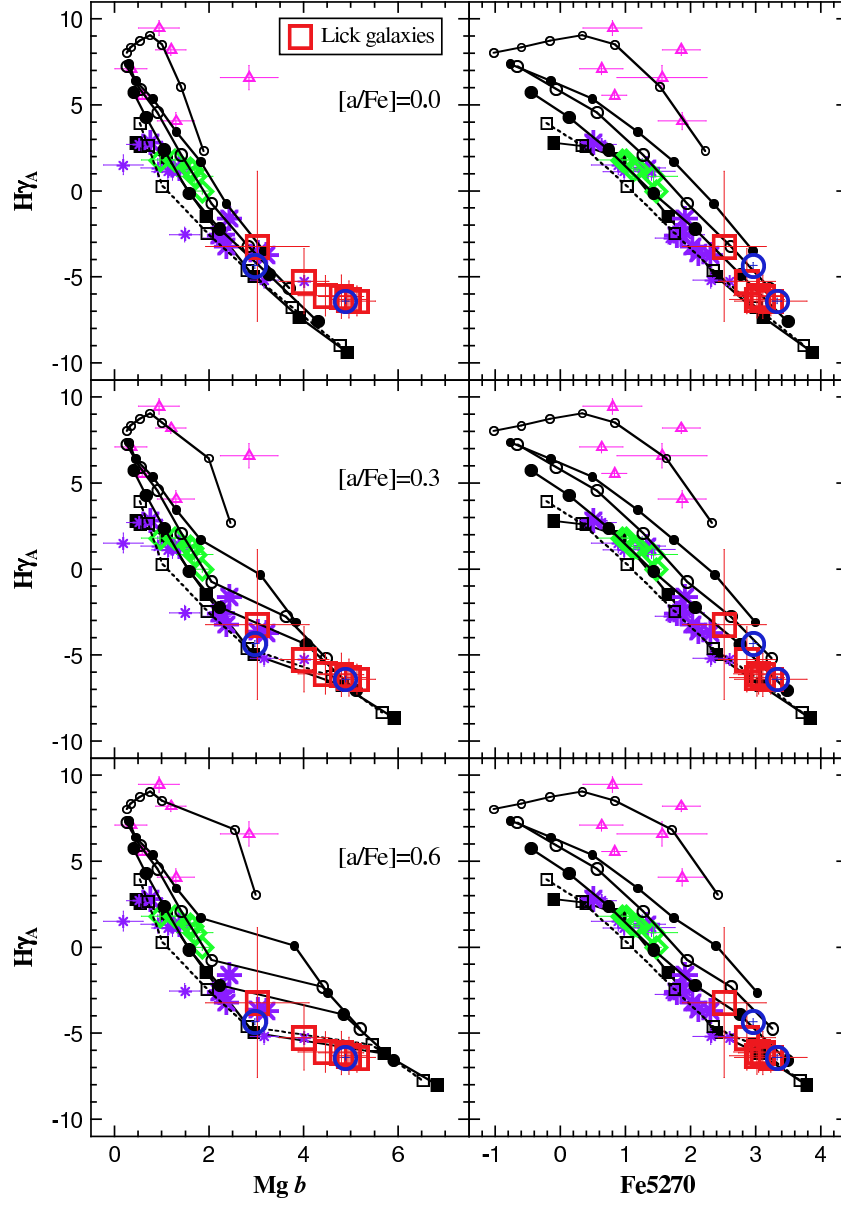


Fig. 14.— Same as Figure 13, but in  $Mg\ b$  vs.  $H\gamma_A$  (left panel) and in  $Fe5270$  vs.  $H\gamma_A$  (right panel). Note that  $H\gamma_A$  is significantly affected by  $\alpha$ -enhancement and results in widely different age and metallicity estimation, especially in the left panel.

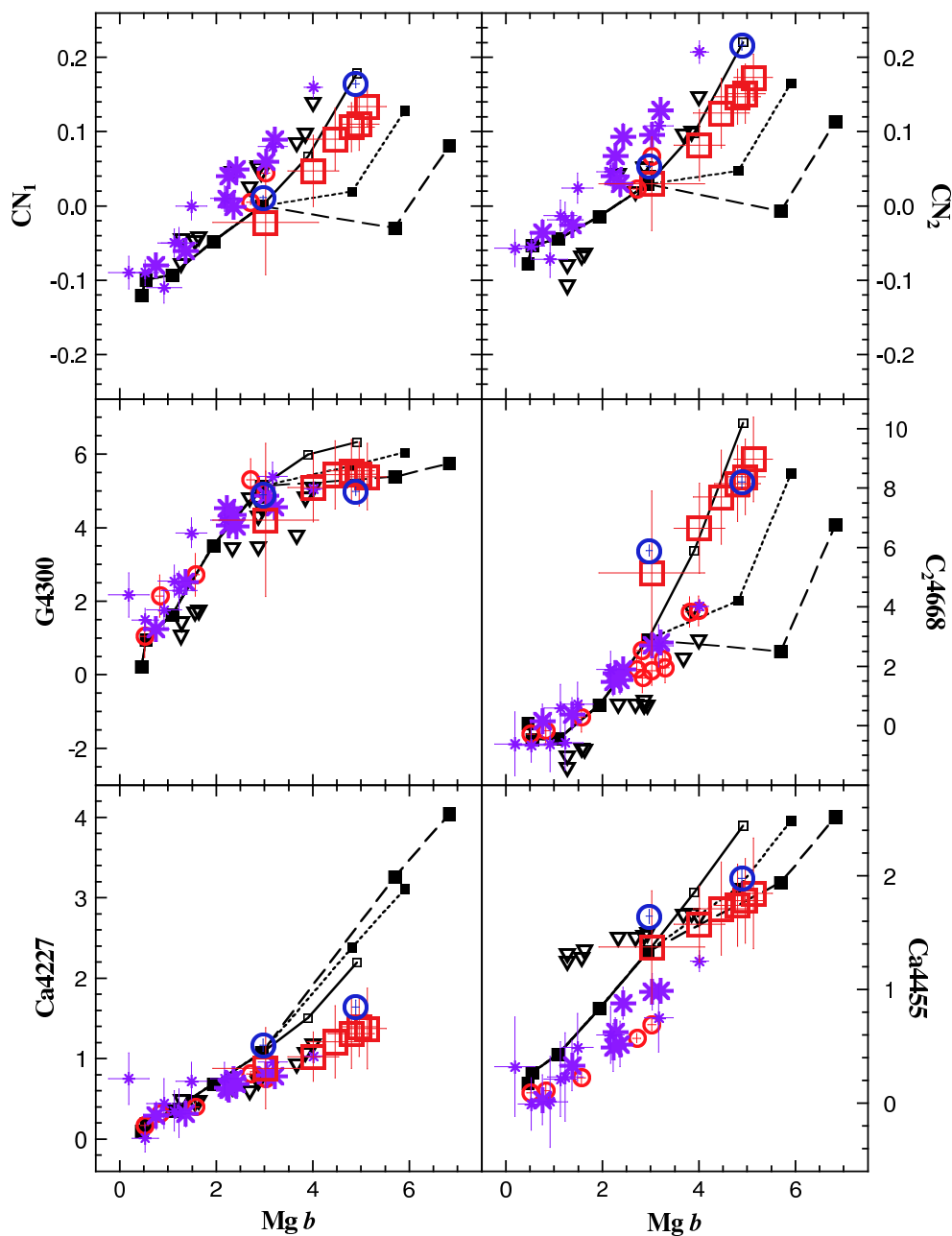


Fig. 15.— Similar to Figure 10, but with median Lick galaxies (big open squares), M31 (*right big open circle*), and M32 (*left big open circle*) compared with Milky Way GCs, bona fide old M31 GCs, and 12 Gyr models in  $Mg\ b$  vs.  $CN_1$ ,  $CN_2$ ,  $G_{4300}$ ,  $C_{24668}$ ,  $Ca_{4227}$ , and  $Ca_{4455}$ . Cluster symbols are the same as in Figures 3 and 7.

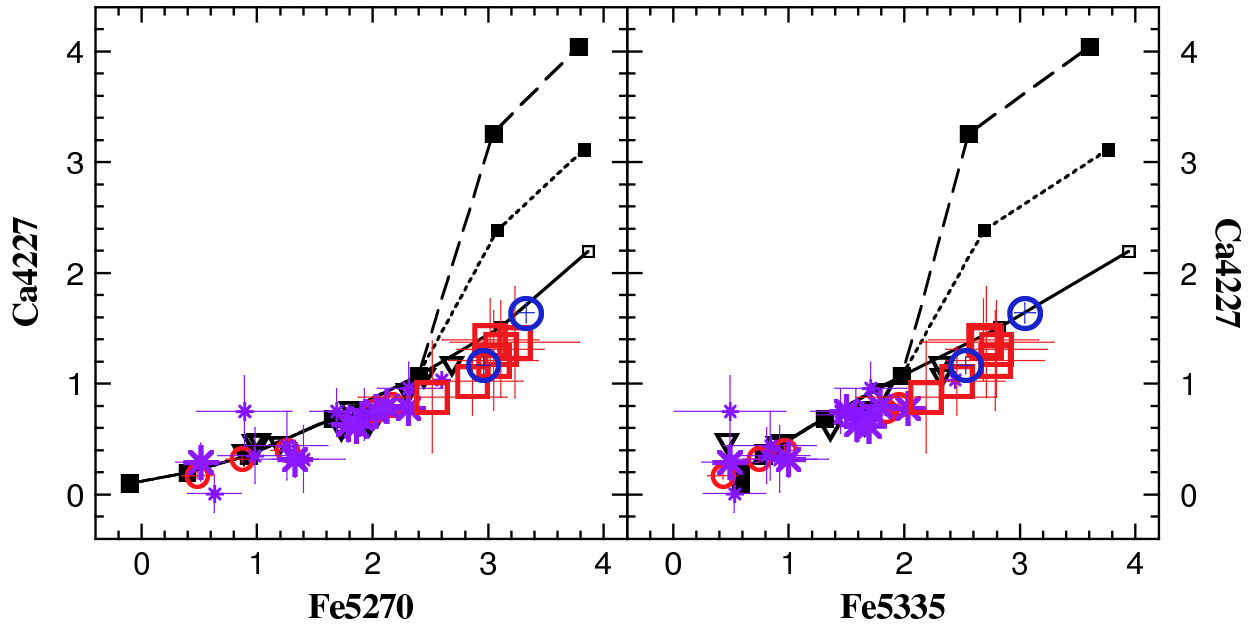


Fig. 16.— Similar to the bottom left of Figure 15, but Ca4227 vs. Fe5270 (left) and Fe5335 (right). Note that the Ca underabundance is not outstanding in these plots.

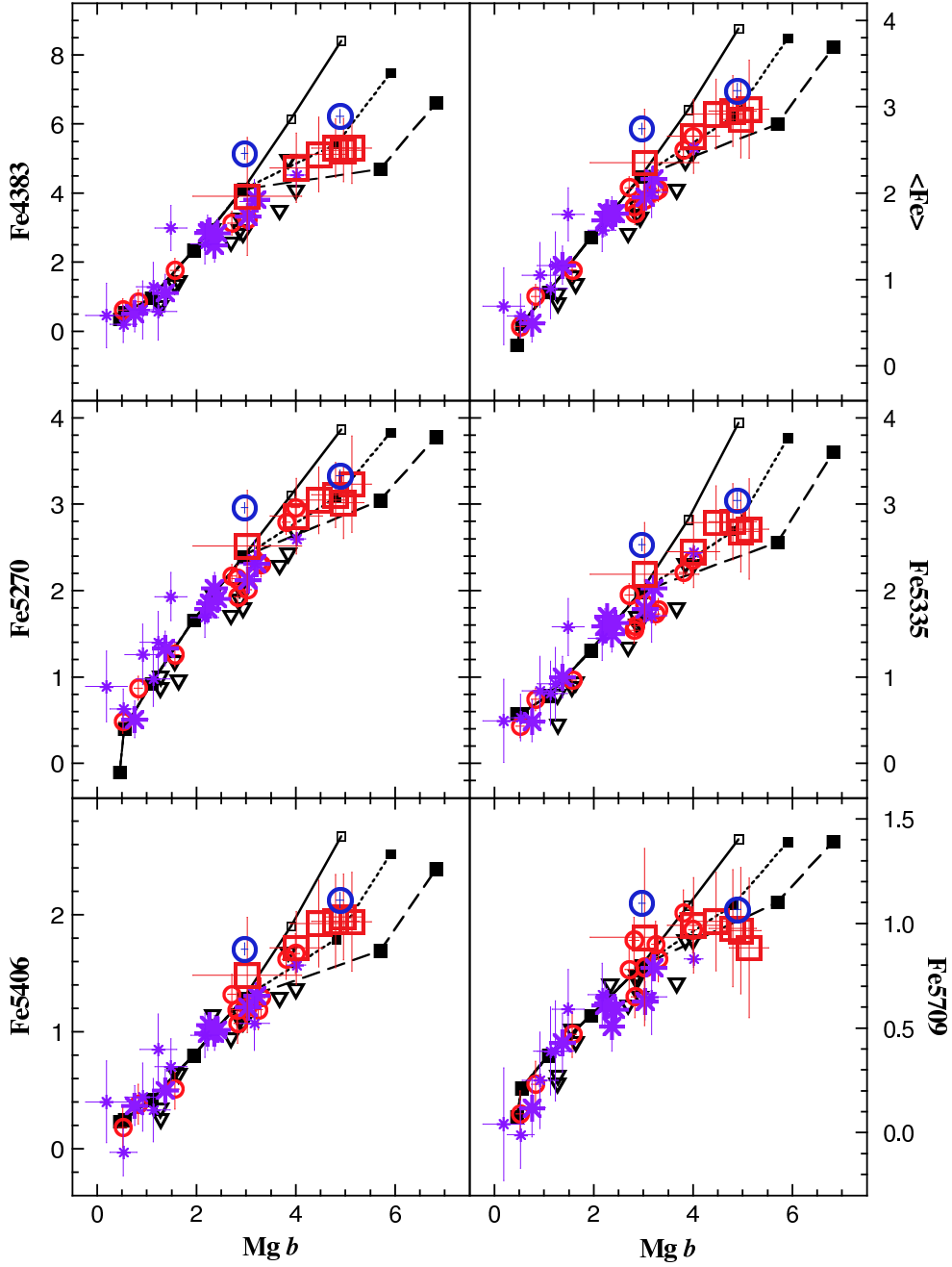


Fig. 17.— Similar to Figure 11, but with median Lick galaxies (big open squares), M31 (*right big open circle*), and M32 (*left big open circle*) compared with Milky Way GCs, bona fide old M31 GCs, and 12 Gyr models in  $\text{Mg } b$  vs. Fe4383,  $\langle \text{Fe} \rangle$ , Fe5270, Fe5335, Fe5406, and Fe5709. Cluster symbols are the same as in Figures 3 and 7.

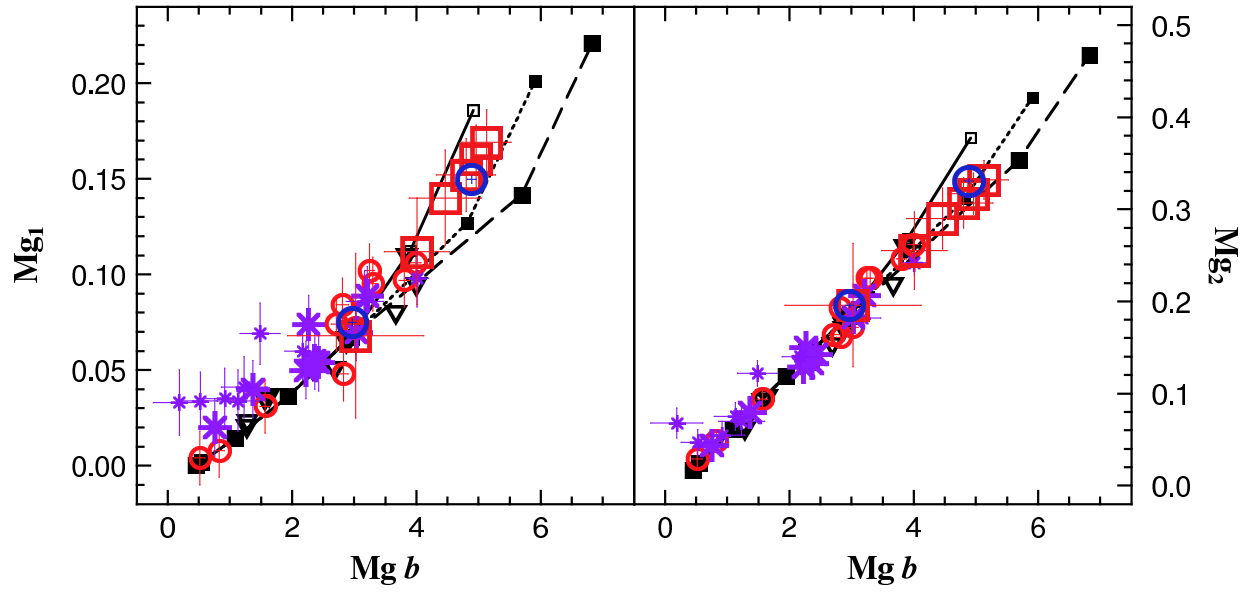


Fig. 18.— Similar to Figure 5. Galaxies, Milky Way GCs, and bona fide old M31 GCs are compared with 12 Gyr models in  $Mg\ b$  vs.  $Mg_1$  and  $Mg_2$ . Symbols are the same as in Figures 3, 7, and 13.

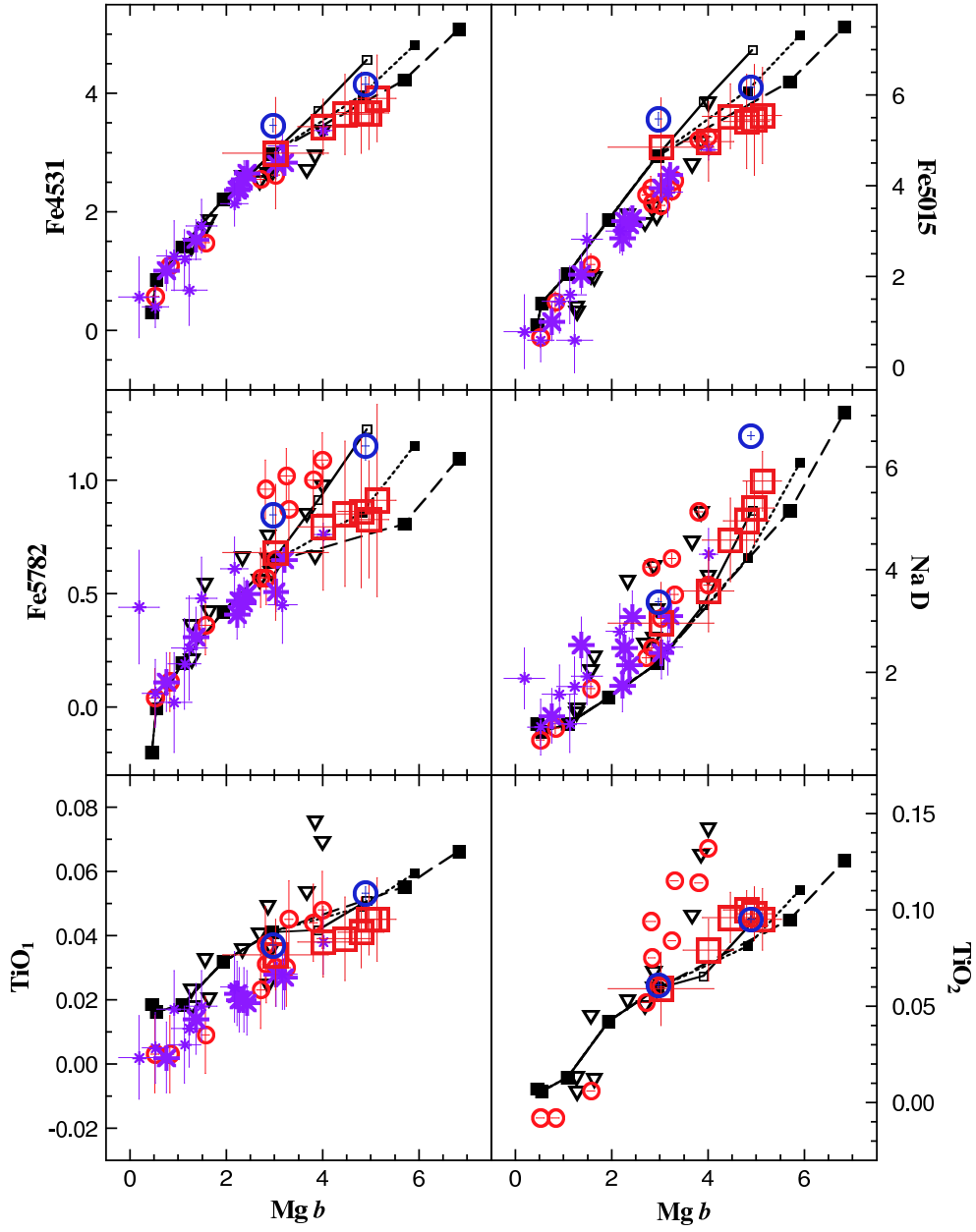


Fig. 19.— Similar to Figure 12. Galaxies, Milky Way GCs, and bona fide old M31 GCs are compared with 12 Gyr models for  $Mg\ b$  vs.  $Fe4531$ ,  $Fe5015$ ,  $Fe5782$ ,  $Na\ D$ ,  $TiO_1$ , and  $TiO_2$ . Symbols are the same as in Figures 3, 7, and 13.